Low Carbon n-GaN Drift Layers for Vertical Power Electronic Devices

Eric Carlson

Dissertation submitted to the faculty of the Virginia Polytechnic Institute and State University in partial fulfillment of the requirements for the degree of

Doctor of Philosophy in Materials Science and Engineering

Lou J. Guido, Chair

William T. Reynolds

Guo-Quan Lu

Carlos T.A. Suchicital

Khai D. T. Ngo

May 8, 2023

Blacksburg, VA

Keywords: Gallium Nitride, Power Electronics, MOCVD, epitaxial growth, III-V Semiconductors, pn diode, carbon impurities, point defects

Copyright, 2023 Eric Carlson

Low Carbon n-GaN Drift Layers for Vertical Power Electronic Devices

Eric Carlson

Dissertation Abstract

GaN holds significant potential as a material for vertical p-n diodes, enabling the realization of devices with reverse breakdown voltages of 5 kV or higher. Carbon serves as the primary compensating dopant in the growth process, incorporated into GaN during metalorganic chemical vapor deposition (MOCVD) growth. The level of carbon incorporation depends on several factors, including growth rate, ammonia flow, temperature, pressure, and trimethylgallium (TMGa) flow. Through guided empirical modeling, it was demonstrated that the carbon incorporation in GaN growth could be predicted using a single parameter based on the ratio of ammonia flow to the growth rate. This model accurately predicts carbon concentrations ranging from $1x10^{17}$ to $5x10^{14}$ cm^{-3} while allowing for maximized growth rates. Other extrinsic dopants have either been reduced below the threshold of consideration or modeled using similar single-parameter relationships. By identifying the dominant extrinsic dopants and accounting for them, an intrinsic defect with a concentration of $2.2x10^{15}$ cm^{-3} was identified. By combining these relationships, growth conditions for n-GaN were optimized, resulting in electron concentrations as low as $1x10^{15}$ cm^{-3}. Leveraging these techniques, p-n diodes were grown, achieving a reverse breakdown voltage as high as 3.1 kV.

Low Carbon n-GaN Drift Layers for Vertical Power Electronic Devices

Eric Carlson

General Audience Abstract

Power electronic devices based on vertical GaN have the potential to revolutionize applications such as electric vehicles, solar charging systems, and the smart grid. However, there are significant materials challenges that need to be addressed to implement these devices. They must be extremely pure and extremely thick to achieve the electrical properties desired. Unfortunately, the primary source for thin film growth of these materials also contains carbon, which can negatively impact purity. To overcome this challenge, an empirical model for the growth process has been developed. This model enables independent control over the carbon source and the removal of carbon, using a single parameter. By leveraging this model, it becomes possible to optimize the trade-off between high purity, high growth rates, and ideal electronic properties. Using these techniques, devices were grown with next-generation levels of performance at minimal time and cost.

Acknowledgements

I would like to extend my sincere appreciation and gratitude to all those who have contributed to making this endeavor possible. First and foremost, I am immensely grateful to Dr. Lou Guido for welcoming me into his research group, despite my non-traditional background in industry. He not only provided me with the opportunity to join his lab but also established an environment conducive to productive work at the exciting intersection of materials and electrical engineering. And, for providing a fun, family-like environment when we weren't working away in the lab. Moreover, I am grateful to Dr. Guido for fostering a supportive and enjoyable atmosphere that felt like a close-knit group, even beyond our lab hours, and for sharing countless memorable stories.

Within the research group, I would like to thank Tim and Noah for being great and interesting lab mates who I could trust to make things work.

I would also like to acknowledge the invaluable support provided by Dr. Khai Ngo, who provided support when things got complicated and made sure I had what I needed to reach the end of my degree. His assistance in critiquing and improving my writing skills was particularly invaluable.

Furthermore, I would like to express my gratitude to the staff at CPES for their patience and support as I navigated the intricacies of a different administrative setup. Their assistance was instrumental in facilitating a smooth transition.

Special thanks go to Dr. Yuhao Zhang and Dr. Ming Xiao for their contributions in fabricating and measuring the diodes for this project. Seeing the actual devices based on the materials I grew before the conclusion of the project was very gratifying.

I am also indebted to the other members of my committee, Dr. Reynolds, Dr. Lu, and Dr. Suchicital, for their valuable guidance and advice in effectively communicating my research results in a clear and focused manner.

I am grateful to the staff in the Materials Science department who provided encouragement and support throughout my journey, helping me navigate the complexities of the university system.

Last but not least, I want to express my heartfelt gratitude to my wife, Kim, whose unwavering support has been a constant source of strength during the various challenges and unpredictable moments encountered along this particular journey.

To each individual mentioned above, and to those whose contributions may not have been explicitly stated, I am sincerely thankful for your support, guidance, and belief in my capabilities.

This work was made possible by funding from the ARPA-E P-N Diodes program and from the Office of Naval Research.

Table of Contents

Abstract ii
General Audience Abstract iii
Acknowledgements iv
Table of Contents vi
List of Tables viii
List of Figures ix

1. Introduction 1

1.1. Motivation 1
1.2. Doping 2
1.3. Growth 5
1.4. Mechanistic modeling 8
1.5. Experimental measurements 9
1.6. Conclusion 11
References 12

2. Control of carbon concentration with ammonia flow 15

2.1. Experimental setup 15
2.2. Stable high ammonia growth conditions 17
2.3. Reducing process parameters 21
2.4. Carbon incorporation vs temperature 23
2.5. Carbon incorporation vs growth rate 26
2.6. Conclusions 27
References 31

3. Additional extrinsic dopants and compensators. 32

3.1. Silicon 32
3.2. Unintentional Fe doping 34
3.3. Unintentional oxygen doping 39
3.4. Intentional Mg doping 40

3.5. Conclusions....41
References....43

4. Electronic properties 44

4.1. Using the model....44
4.2. Experimental....45
4.3. Heteroepitaxial growth on GaN templates....45
4.4. Homoepitaxial growth on HVPE GaN....47
4.5. p-n diode growth....50
4.6. Conclusions....51
References....53
List of Publications and Conference Presentations....54

List of Tables

Table 1.1 - Process inputs that lead to decreased carbon concentrations. 10

Table 2.1 – Reactor Flow conditions. All flow values in the table are sccm................................17

Table 2.2 – Apparent activation energies. 26

Table 2.3 – Carbon incorporation fit data. 28

Table 2.4 – Reactor styles in references. 29

Table 3.1 – Wafer Cleaning Procedures. 36

Table 3.2 – Steps in the handling/cleaning experiment. 36

Table 4.1 – Model calculations for 5kV n-GaN drift layer...50

List of Figures

Figure 1.1 – Typical vertical GaN device structure. 1

Figure 1.2 – Reverse breakdown voltage of a GaN p-n diode. n is the electron concentration.......2

Figure 1.3 – Potential dopants and defects in MOCVD GaN with approximate ionization energies. 4

Figure 1.4 – Three growth regimes 1) kinetically limited, 2) mass transport-limited, 3) desorption limited. [19]...7

Figure 1.5 – Carbon incorporation from literature versus a) temperature, b) reactor pressure, c) ammonia flow from Koleske[29], He[30], Danielsson[20], Chen[31]. Hollow data points are below the SIMS detection limit. 10

Figure 2.1 Aixtron 200/4 RF-S growth region schematic...16

Figure 2.2 - Unstable growth rate relations. The points are connected in the order grown. The detailed gas flow conditions for each trace can be found in Table 2.1. 18

Figure 2.3 – Linear growth rate relations for reactor flow conditions used for SIMS measurements. 19

Figure 2.4 - Growth rate measured across a range of ammonia flow and carrier gas mixes. The gas mix goes from 92% hydrogen in a balance of NH_3 to 15% hydrogen. The dashed line the calculated diffusion of TMGa in a H_2/NH_3 gas mixture. 20

Figure 2.5 – SIMS depth profile showing O, Si, and C concentrations..21

Figure 2.6 – Carbon concentration from SIMS a) versus TMGa flow, b) Versus ammonia flow with a fixed growth rate of 1.5 µm/hr and variable TMGa flow. 22

Figure 2.7 – Carbon concentration from SIMS a) versus V/III ratio, b) versus ammonia flow/growth rate...23

Figure 2.8 - Incorporation of carbon with respect to ammonia flow and temperature. The data point labels indicate the temperature in degrees Celsius. Inset plot shows lower temperature limit to model vs. ammonia flow. 24

Figure 2.9 – Temperature dependence of the growth rate for ammonia flow from 1.3 – 10 slm. The data have been vertically offset for visibility. The dashed lines are drawn to guide the eye. Labels are ammonia flow. 25

Figure 2.10 – a) Carbon concentration normalized by the model curve. The dashed lines are used as guides for the eye to see where the data departs from the model curve. b) Maximum growth rate cutoff values. 27

Figure 2.11 – Carbon concentration for all ammonia flows with temperature and growth rate limits applied. 28

Figure 2.12 – Data from this work compared to previous works with carbon incorporation replotted versus V/GR. The data is from Danielsson[1], Koleske[6], Piao[13], and Kaess[14].

Figure 3.1 – SIMS data at a fixed ammonia flow of 10 slm. 33

Figure 3.2 – Intentional silicon concentration. 34

Figure 3.3 – Unintentional silicon incorporation. Legend is ammonia flow. 35

Figure 3.4 – SIMS analysis for metal contamination. Experiment steps are labeled at bottom. ... 38

Figure 3.5 – SIMS analysis for metal contamination. a) temperature response b) Growth of thick GaN layer on HVPE GaN full wafer. 39

Figure 3.6 – SIMS measurement of C, Si, O, and H for a 10 μm thick sample grown on a full SCIOCS GaN wafer. 40

Figure 3.7 – Magnesium incorporation at 1.3 and 7.8 slm ammonia flow. 41

Figure 4.1 – Plot of the model to choose growth conditions for the desired electron concentration. Ammonia flow a) 1.3 slm, b) 5.2 slm, c) 7.8 slm, d) 10 slm.. 44

Figure 4.2 – Parity plot of carbon incorporation in GaN on sapphire. The solid points are raw model estimates of electron concentrations, and the hollow points are the estimate with an additional $4x10^{15}$ cm^{-3} of compensation added. 46

Figure 4.3 – Parity plot for samples growth on HVPE GaN substrates. The solid points are raw model estimates of electron concentrations, and the hollow points are the estimate with an additional $2.2x10^{15}$ cm^{-3} of compensation added. 47

Figure 4.4 – Plot of adjusted model to use to choose growth conditions for the desired electron concentration with 50% compensation. Ammonia flow a) 1.3 slm, b) 5.2 slm, c) 7.8 slm, d) 10 slm. 48

Figure 4.5 – Electron concentrations extracted from Hg Probe C-V. GaN on GaN homoepitaxy. a) uneven electron concentration at 90% compensation, b) good electron concentration profile at a maximum of 76% compensation. 49

Figure 4.6 – a) p-n device structure schematic and b) measured reverse breakdown voltage of fabricated device. 50
Figure 4.7 – Model calculation for maximum growth rate. 51

Chapter 1 Introduction

1.1 Motivation

Power electronic devices are currently in high demand for power conversion applications in solar and wind power, variable frequency motor drives, naval electronics, and electric vehicles. These devices are currently available based on silicon, and more recently SiC technology. Gallium nitride (GaN) holds promise for the next generation of devices. As an example, for applications for low-frequency vertical power switches, the Baliga figure of merit has been defined by Baliga [1] as $\mathrm{BFOM} = \epsilon\mu E_c^3$. The BFOM for Silicon, SiC, and GaN are respectively, 1, 190 and 850. The high critical breakdown field of GaN, E_c, is mostly responsible for this performance.

Currently, the most promising GaN devices are being designed in a vertical configuration to produce compact, high-power capability. A typical simplified configuration is shown in Figure 1.1.

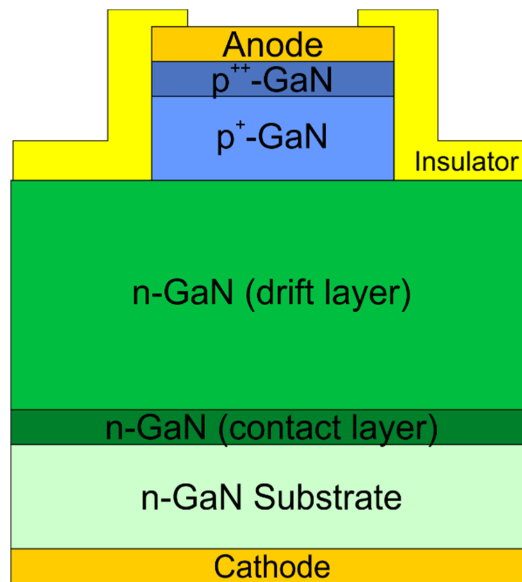

Figure 1.1 – Typical vertical GaN device structure.

The n-GaN drift layer is a crucial element in this structure, affecting two critical device parameters: reverse breakdown voltage (V_B) and on state resistance (R_{ON}). Achieving a high V_B requires the voltage drop in this layer to be spread out with a low electron concentration (n), which prevents exceeding the fundamental breakdown strength of GaN. This allows the depletion width in the drift layer to span the entire layer thickness of up to tens of microns. Maintaining a low

R_{ON} necessitates controlling the electron concentration to these low levels with minimum compensation. Unintentional dopants must have a concentration of a fraction of the desired electron concentration to achieve this. These unintentional dopants, besides preventing the ideal electron concentration from being reached, can also increase the reverse leakage current, reduce V_B, and decrease electron mobility. Currently, the state of the art is a V_B of around 3 kV [2], [3]. Figure 1.2 shows the relationship between the thickness of the drift layer, the electron concentration, and V_B. A V_B of as high as 20 kV is possible if n can be controlled into the low 10^{15}s. The goal of this technology is a V_B of 5 kV, with up to 20 kV as an ultimate target. To achieve a V_B of 5 kV and beyond, electron concentrations with minimal compensation around 3×10^{15} cm^{-3} must be attained.

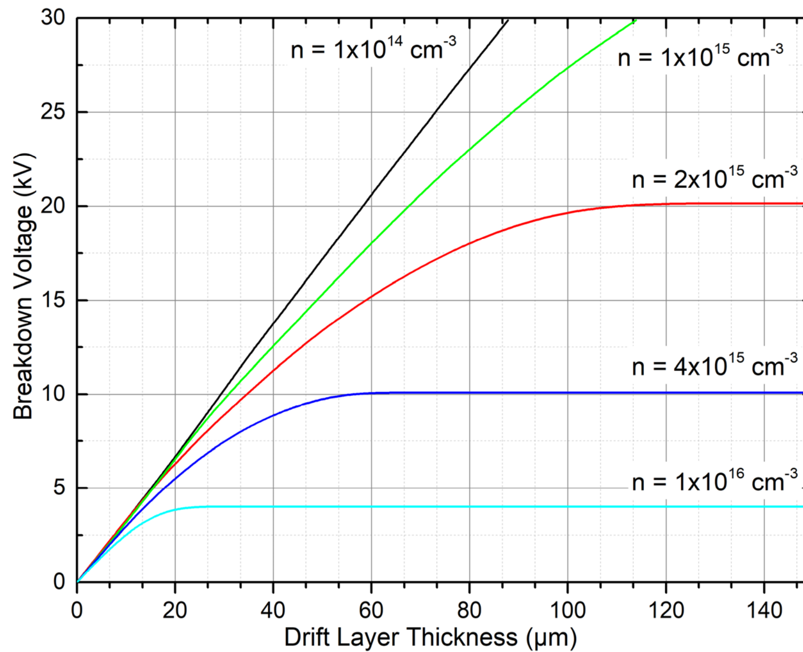

Figure 1.2 – Reverse breakdown voltage of a GaN p-n diode. n is the electron concentration.

1.2 Doping

The drift layer in this device structure is n-type with electrons serving as the majority carriers. Pure GaN is an insulator, so donor atoms like silicon must be introduced to enable electron conduction. The source of silicon donors in metalorganic chemical vapor deposition (MOCVD) is silane gas (SiH_4). Ideally, each silicon atom would contribute a conduction electron, and the total electron concentration would equal the silicon concentration. However, in real-world material,

unintentional dopants can contaminate the material and affect the total number of electrons available for conduction.

Dopants in GaN fall into roughly three categories: shallow donors, shallow acceptors, and deep traps. Shallow donors donate most of their electrons to the conduction band at room temperature. In n-type material, shallow acceptors capture electrons from the valence band, reducing the overall electron concentration available for conduction. Deep traps can capture electrons from the shallow donors and the conduction band, a process known as compensation, resulting in a decrease in the total electron concentration.

Dopants can be intentional dopants (ID) or unintentional dopants (UID). Silicon is an example of an intentional dopant in GaN. Unintentional dopants, on the other hand, can manifest in various forms, including native defects like vacancies, V_{Ga}, and V_N, anti-site defects, interstitials, and complexes. Directly measuring these defects can be challenging; however, their effects can be detected through electrical and optical means. Unintentional dopants can also arise from extrinsic sources such as contaminants in the growth sources, environmental contamination, and reactor components. These defects may exist in isolation, be combined together as complexes, or be associated with surfaces or dislocations.

In the nomenclature used for dopants and defects in semiconductors, the capital letter represents the dopant atom or, in the case of a vacancy, the letter “V”. The subscript indicates the specific location of the dopant or defect within the crystal structure. In the context of GaN, the sublattices consist of Ga and N atoms, while the interstitial sites between the lattice are represented by the letter "I."

A dominant native defect may be a gallium vacancy, V_{Ga} [4], which can compensate electrons. Concentrations of gallium vacancies as high as $1x10^{19}$ cm^{-3} have been measured using positron annihilation spectroscopy, especially at high V/III ratios[5]–[7]. However, more recent work recalculating formation energies claims V_{Ga} as unlikely but could be significant in the form of complexes[8]. A trap located at E_C-0.6 eV has been identified[9] and associated with a nitrogen anti-site defect, N_{Ga}[10], [11], however Van de Walle[4] claims it is unlikely due to an unfavorable formation energy. In materials with a high dislocation density, V_{Ga} or V_N is suspected to decorate the dislocations producing a range of compensating defect states. [12]–[14]

The extrinsic UIDs can be divided up into electron donors and compensators. Silicon, a donor, is known to be a small contaminant in some growth sources as well as a component of the quartz and SiC components in the reactor that are at high temperature. Oxygen is another shallow donor that is endemic in the growth process. It is suspected that oxygen is the source of n-type growth in nominally UID material that plagued GaN growth in the early years of development. It may come from growth sources as well as atmospheric sources. Compensating sources include, in terms of extrinsic compensators, transition metals of which Fe and Cr are potential sources. Fe has been used to produce insulating layers and has been found to contaminate GaN growth[15], [16]. The main UID contaminant in MOCVD Growth of GaN is carbon and can easily be seen in concentrations up to 1×10^{18} cm^{-3} under typical growth conditions. The origin of this is the source of Ga, Trimethylgallium (TMGa, $Ga(CH_3)_3$) with its three carbons. For n-type material the carbon is predicted to have the lowest formation energy on a nitrogen site, C_N. [4] The most recent DFT calculations have determined that C_N is a deep acceptor with a (0/-) transition level at $E_V + 0.9\ eV$. [17] This is ideal for compensating electrons. A schematic of the possible defects and dopants in GaN is shown in Figure 1.3.

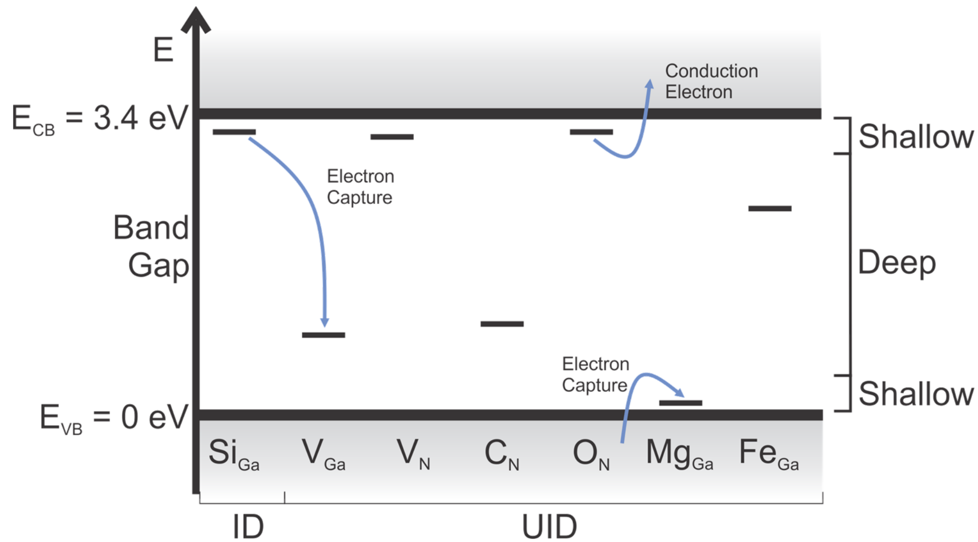

Figure 1.3 – Potential dopants and defects in MOCVD GaN with approximate ionization energies.

The total electron concentration available for conduction can be calculated by subtracting the total concentration of compensating traps and shallow acceptors from the total concentration of shallow donors. However, this assumes that all states are fully ionized, which is not strictly the case. If the difference between the two concentrations is small, the resulting electron concentration would be

low, which is not desirable. Additionally, small variations in either concentration would lead to significant fluctuations in the electron concentration. Small variations will always be observed from sample to sample and across the substrates. Moreover, increasing compensation has been shown to decrease mobility sharply[18], leading to a reduction in R_{ON} in diodes constructed from this material. Thus, the ultimate goal is to minimize compensation by reducing the concentration of unintentional dopants and defects as much as possible.

1.3 Growth

The growth of GaN using metal-organic chemical vapor deposition (MOCVD) involves multiple steps and will include reactions in both the gas phase and on the substrate surface, with potential impacts from the gas phase and surface diffusion. The process is activated when the source and carrier gases encounter the hot substrate region. The process can be broken up into these steps:

1. Gas phase transport
2. Diffusion across the boundary layer.
3. Adsorption/chemisorption at the surface
4. Reaction/decomposition on the surface
5. Surface diffusion across the terraces
6. Incorporation at the step edge

Gas phase reactions can occur in the first two steps, and also with adsorbed molecules as well. The desorption of any of the components on the surface and step edges will occur in parallel with adsorption, reaction, and incorporation on the step edges.

The relationship between the concentration of each component at the growing surface and the concentration in the bulk gas is influenced by several factors including the thickness of the boundary layer, the diffusion rate across the boundary layer, and the rate of surface reactions. The flux to the surface, step 2, is

$$F = k_g[(bulk\ gas\ concentration) - (concentration\ at\ surface)] \quad (1)$$

Adding the next two steps

$$Growth\ Rate = \frac{P^{\circ}}{\frac{1}{k_f} + \frac{1}{k_g}(1 + \frac{1}{K})} \quad (2)$$

P° is the partial pressure in the gas flowing above the boundary layer, k_g is the diffusion constant through the boundary layer, k_f is the forward surface reaction rate constant which is proportional to $Ae^{-\frac{E_A}{RT}}$, and K is the reversible surface reaction constant. The diffusion constant, k_g, is a function of the boundary layer thickness, δ, and the gas diffusion constant, D,

$$k_g = D/\delta \quad (3)$$

with

$$D \propto T^{3/2} \quad (4)$$

$$\delta(x) \approx 5\sqrt{\frac{x\eta}{v_0\rho}} \quad (5)$$

Where x is the distance along the substrate in the direction of gas flow, η is the dynamic viscosity, ρ is the gas density, and v_0 is the gas velocity above the boundary layer.

The determination of surface concentrations is challenging due to the combined effects of surface reaction rates and gas diffusion rates, which are influenced by various factors such as temperature, flow velocity, pressure, gas mix, and reactor geometries. In modeling the growth process, calculating surface concentrations is a crucial initial step before addressing surface reactions, surface diffusion, and incorporation mechanisms. The complexity is further amplified by the diverse conditions and reactor geometries encountered. However, the flux can be directly determined from the growth rate, making it a comparatively straightforward parameter to measure.

A typical chemical vapor deposition (CVD) reactor has a temperature response that is indicative of the limiting part of the process. At low temperatures, the reaction rate increases strongly with temperature, indicating an activated, kinetically limited process. The rate-determining step in this case is the adsorption and reaction of adsorbed molecules. The gas concentration at the surface will be closer to that in the bulk gas.

At higher temperatures, the response to temperature is weaker, indicating a mass transport-limited process. In this regime, the flux of molecules to the surface will be a function of the boundary layer

diffusion. The diffusion process depends on factors such as the gas mix, flow velocity, gas density, and, to a lesser extent, temperature. Consequently, the concentration of the source gas at the surface becomes very low. The growth rate in this regime is determined by the flux of molecules reaching the surface.

At the highest temperatures, the growth rate decreases with increased temperature, indicating that desorption from the surface is becoming a dominant factor. In this regime, desorption plays a crucial role in the overall process.

Figure 1.4 from Mihopoulos[19] provides a comprehensive illustration of these three growth regimes, presenting both experimental and calculated data. In this figure, the mass transport-limited growth regime spans from 600 to 1000°C with the kinetic and desorption limited regimes below and above this range, respectively.

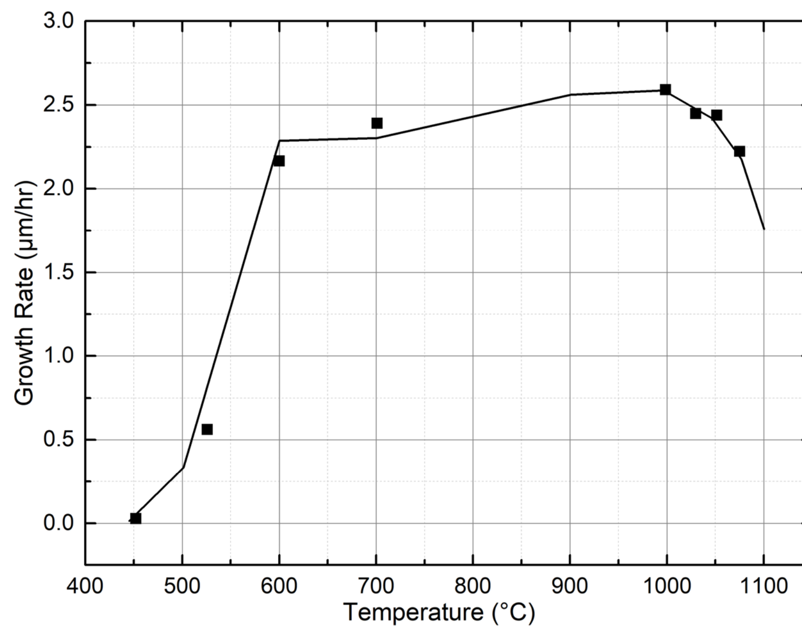

Figure 1.4 – Three growth regimes 1) kinetically limited, 2) mass transport-limited, 3) desorption limited. [19]

In research and production, several different reactor geometries are found. The close-coupled showerhead (CCS) reactor has a large number of small nozzles very close to the substrates that inject source gases down onto the top surface of the wafer(s). A vertical laminar flow reactor injects the gas into the center of a rotating susceptor containing the wafers and exits at the edges of the susceptor. The gas flows in a laminar manner across the wafers. In contrast, the horizontal

reactor, which was employed in this particular study, involves gas injection from one side of a rotating wafer, flowing across the wafer, and exiting from the opposite side. Both the vertical and horizontal reactors achieve a laminar flow pattern as the gas traverses the wafer surface.

Due to the challenges associated with directly observing the reaction components present in the gas or on the surface, experimental investigations are often limited to in situ measurements of gas inputs, pressure, temperature, and growth rates. These parameters provide valuable insights into the process dynamics without requiring direct observation of the reaction components themselves.

1.4 Mechanistic modeling

It would be a great help in producing low-carbon material if an existing mechanistic model could be used as a guide for growth conditions. Several groups have attempted to model the basic growth process as well as carbon incorporation. The models generally cover only a subset of the growth steps listed above. Most start with the gas pressures directly at the surface and do not attempt to model the diffusion process and gas flow. Some do cover this step but either exclude or assume the surface reactions and diffusion to be insignificant. There is also little agreement as to the specific molecules that reach the surface to supply Ga, N, and the source of carbon. A few example models will be discussed.

Some literature [20]–[22] proposes a reaction of the form

$$Ga(CH_3)_{x(g)} + NH_{y(g)} \rightarrow Ga(CH_3)_{x-1(ads)} + NH_{y-1(ads)} + CH_{4(g)} \quad (6)$$

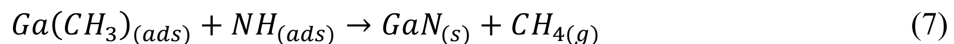

$$Ga(CH_3)_{(ads)} + NH_{(ads)} \rightarrow GaN_{(s)} + CH_{4(g)} \quad (7)$$

The Ga metalorganic (TMGa) does decompose in the gas partially with most reaching the surface as monomethylgallium (MMGa). NH_3 has a very slow decomposition rate in the gas at these temperatures due to its high activation energy, so it mostly reaches the surface unchanged as NH_3 [23], [24]. It then follows a stepwise decomposition as NH_3->NH_2->NH->N[21], [23], [25]. The surface adsorbed Ga and N diffuse to step edges and incorporate into the growing film. The H atoms produced from the decomposition of NH_3 can recombine with NH_x and desorb as NH_3 or combine with CH_3 left from the MMGa and desorb as relatively inert CH_4.

Other groups [18], [26]–[28] assume a completely homogenous gas phase reaction in which the TMGa is completely decomposed in the gas and only Ga atoms reach the surface to incorporate.

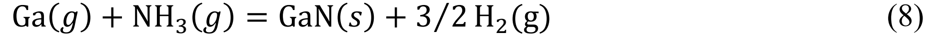

$$Ga(g) + NH_3(g) = GaN(s) + 3/2\, H_2(g) \quad (8)$$

This also represents the simplest reaction equation to generate an equilibrium pressure of the reactants used to generate a driving force for the reaction. Assuming equilibrium for an equation like this would require operating in a mass transport-limited mode with fast surface reactions. Using this equation presupposes that all carbon is removed from the metalorganic in the gas and arrives at the growing surface in a variety of hydrocarbon forms including CH_4, C_2H_4, C_2H_2, C_2H_6, and others. Other possible chemistries include GaH as the gallium source [28].

Due to the inherent challenges in directly measuring the gas phase or surface chemistry, the majority of intermediate steps in the models are purely theoretical. Consequently, the theoretical results can only be compared to the outcomes obtained from experimental measurements. Attempting to precisely match the detailed conditions within the reactor is not pursued due to these limitations.

While there are techniques to do this, the geometry of actual reactors make these measurements difficult and rare. Mazzarese performed one of the limited direct measurements of the chemistry of the gas phase [22]. Using FTIR and isotopically labeled ND_3 they were able to determine that the majority of the methane produced during growth was a result of a surface reaction between the CH_3 radicals from the metalorganic and the deuterium from the ammonia, forming CH_3D.

Matching actual carbon incorporation data using models often requires the utilization of numerous adjustable parameters, and even then, achieving a close approximation to experimental results can be challenging. When considering an arbitrary reactor and growth conditions, the modeling process offers limited assistance in accurately predicting and controlling carbon incorporation with specific reactor conditions.

1.5 Experimental Measurements

In terms of practical suggestions to lower carbon incorporation, the experimental literature can provide some direction. Figure 1.5 shows the response of carbon incorporation to process inputs from several research groups.

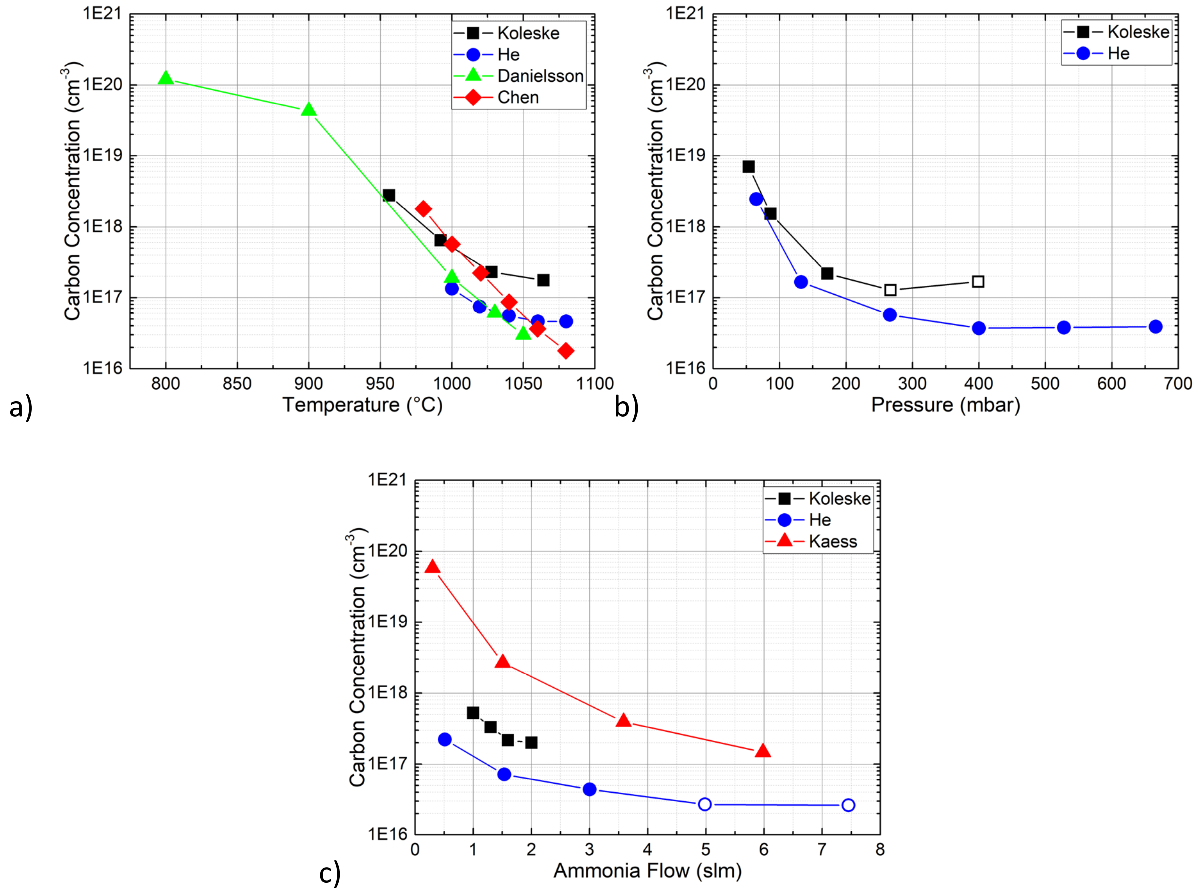

Figure 1.5 – Carbon incorporation from literature versus a) temperature, b) reactor pressure, c) ammonia flow from Koleske[29], He[30], Danielsson[20], Chen[31]. Hollow data points are below the SIMS detection limit.

The trends extracted from the literature are listed in Table 1.1.

Table 1.1 Process inputs that lead to decreased carbon concentrations.

Increase	**Decrease**
Ammonia flow	Growth Rate
V/III ratio	
Pressure	
Temperature	

Trying to compare the experimental data beyond general trends is difficult. Each experiment holds different parameters fixed while changing others. Because the process parameters are not always independent of each other the relation between carbon incorporation and a specific parameter can

be incomplete. As a specific example, growth rate is impacted by temperature, pressure, and for some reactors, ammonia flow. Growth rate is inherently tied to carbon incorporation because a portion of the Ga atoms reaching the surface are still bonded to one or more methyl groups[20].

1.6 Conclusion

To tackle the challenge of reducing carbon concentration in GaN MOCVD films, researchers have employed various approaches, including the development of mechanistic models and extensive experimental trials aimed at identifying trends. However, due to the inherent complexity of the growth process, these models often simplify the process to make it more manageable, or they involve a multitude of intricate steps that are challenging to correlate with specific experimental conditions. Consequently, these models typically require multiple independent adjustable parameters to align with experimental data, making it difficult to utilize them for precise predictions.

On the other hand, experimental investigations have successfully identified trends concerning intensive properties like temperature and total pressure, as well as extensive properties related to the source flows. However, the experimental work falls short in addressing the specific control of dopants (donors and acceptors) necessary to finely tune electron concentrations and compensation ratios. Furthermore, a method for achieving precise control consistently across different conditions to attain the lowest carbon concentrations, resulting in the lowest electron concentration and compensation, has not been established.

To achieve precise control over carbon incorporation during the growth of device layers, it would be beneficial to develop a guided empirical model that provides a straightforward mathematical relationship involving a minimal number of parameters within the desired doping range. By establishing fixed relationships among parameters directly related to carbon supply and carbon removal, the complexity of the model can be reduced, thereby decreasing the number of degrees of freedom. Additionally, if other properties, especially the extensive properties, can be maintained constant within the doping range of interest, it would eliminate the need for additional parameters. Simplifying the prediction of carbon incorporation would facilitate the identification of the effects of other extrinsic and intrinsic dopants, enabling better understanding and control of the overall doping process.

References

[1] B. J. Baliga, "Semiconductors for high-voltage, vertical channel field-effect transistors," *Journal of Applied Physics*, vol. 53, no. 3, pp. 1759–1764, Mar. 1982, doi: 10.1063/1.331646.

[2] I. C. Kizilyalli, A. P. Edwards, H. Nie, D. Bour, T. Prunty, and D. Disney, "3.7 kV Vertical GaN PN Diodes," *IEEE Electron Device Letters*, vol. 35, no. 2, pp. 247–249, Feb. 2014, doi: 10.1109/LED.2013.2294175.

[3] K. Nomoto *et al.*, "GaN-on-GaN p-n power diodes with 3.48 kV and 0.95 mΩ-cm2: A record high figure-of-merit of 12.8 GW/cm2," in *2015 IEEE International Electron Devices Meeting (IEDM)*, Dec. 2015, p. 9.7.1-9.7.4. doi: 10.1109/IEDM.2015.7409665.

[4] C. G. Van de Walle and J. Neugebauer, "First-principles calculations for defects and impurities: Applications to III-nitrides," *Journal of Applied Physics*, vol. 95, no. 8, pp. 3851–3879, Mar. 2004, doi: 10.1063/1.1682673.

[5] K. Saarinen *et al.*, "Gallium vacancies and the growth stoichiometry of GaN studied by positron annihilation spectroscopy," *Appl. Phys. Lett.*, vol. 73, no. 22, pp. 3253–3255, Nov. 1998, doi: 10.1063/1.122735.

[6] L. V. JØrgensen, A. C. Kruseman, H. Schut, A. V. Veen, M. Fanciulli, and T. D. Moustakas, "Investigation of Vacancies in GaN by Positron Annihilation," *MRS Online Proceedings Library (OPL)*, vol. 449, p. 853, ed 1996, doi: 10.1557/PROC-449-853.

[7] P. Bogusl/awski, E. L. Briggs, and J. Bernholc, "Native defects in gallium nitride," *Phys. Rev. B*, vol. 51, no. 23, pp. 17255–17258, Jun. 1995, doi: 10.1103/PhysRevB.51.17255.

[8] J. L. Lyons and C. G. Van de Walle, "Computationally predicted energies and properties of defects in GaN," *npj Comput Mater*, vol. 3, no. 1, Art. no. 1, Mar. 2017, doi: 10.1038/s41524-017-0014-2.

[9] T. Narita *et al.*, "Overview of carrier compensation in GaN layers grown by MOVPE: toward the application of vertical power devices," *Jpn. J. Appl. Phys.*, vol. 59, no. SA, p. SA0804, Nov. 2019, doi: 10.7567/1347-4065/ab4610.

[10] D. Haase *et al.*, "Deep-level defects and n-type-carrier concentration in nitrogen implanted GaN," *Applied Physics Letters*, vol. 69, no. 17, pp. 2525–2527, Oct. 1996, doi: 10.1063/1.117727.

[11] T. L. Tansley and R. J. Egan, "Point-defect energies in the nitrides of aluminum, gallium, and indium," *Phys. Rev. B*, vol. 45, no. 19, pp. 10942–10950, May 1992, doi: 10.1103/PhysRevB.45.10942.

[12] S. M. Lee, M. A. Belkhir, X. Y. Zhu, Y. H. Lee, and Y. G. Hwang, "Electronic structures of GaN edge dislocations," *Physical Review B - Condensed Matter and Materials Physics*, vol. 61, no. 23, pp. 16033–16039, 2000, doi: 10.1103/PhysRevB.61.16033.

[13] J. E. Northrup, "Screw dislocations in GaN: The Ga-filled core model," *Applied Physics Letters*, vol. 78, no. 16, pp. 2288–2290, 2001, doi: 10.1063/1.1361274.

[14] A. F. Wright and U. Grossner, "The effect of doping and growth stoichiometry on the core structure of a threading edge dislocation in GaN," *Applied Physics Letters*, vol. 73, no. 19, pp. 2751–2753, 1998, doi: 10.1063/1.122579.

[15] A. Y. Polyakov, N. B. Smirnov, A. V. Govorkov, and S. J. Pearton, "Properties of Fe-doped semi-insulating GaN structures," *Journal of Vacuum Science and Technology B: Microelectronics and Nanometer Structures*, vol. 22, no. 1, pp. 120–125, 2004, doi: 10.1116/1.1633776.

[16] A. Y. Polyakov, N. B. Smirnov, A. V. Govorkov, and S. J. Pearton, "Electrical and optical properties of Fe-doped semi-insulating GaN templates," *Applied Physics Letters*, vol. 83, no. 16, pp. 3314–3316, 2003, doi: 10.1063/1.1621458.

[17] J. L. Lyons, A. Janotti, and C. G. Van de Walle, "Carbon impurities and the yellow luminescence in GaN," *Appl. Phys. Lett.*, vol. 97, no. 15, p. 152108, Oct. 2010, doi: 10.1063/1.3492841.

[18] F. Kaess *et al.*, "Correlation between mobility collapse and carbon impurities in Si-doped GaN grown by low pressure metalorganic chemical vapor deposition," *Journal of Applied Physics*, vol. 120, no. 10, p. 105701, Sep. 2016, doi: 10.1063/1.4962017.

[19] T. Mihopoulos, "Reaction and transport processes in OMCVD : selective and group III-nitride growth," Thesis, Massachusetts Institute of Technology, 1999. Accessed: Mar. 19, 2023. [Online]. Available: https://dspace.mit.edu/handle/1721.1/9655

[20] Ö. Danielsson, X. Li, L. Ojamäe, E. Janzén, H. Pedersen, and U. Forsberg, "A model for carbon incorporation from trimethyl gallium in chemical vapor deposition of gallium nitride," *J. Mater. Chem. C*, vol. 4, no. 4, pp. 863–871, Jan. 2016, doi: 10.1039/C5TC03989D.

[21] Q. An, A. Jaramillo-Botero, W.-G. Liu, and William. A. Goddard, "Reaction Pathways of GaN (0001) Growth from Trimethylgallium and Ammonia versus Triethylgallium and Hydrazine Using First Principle Calculations," *J. Phys. Chem. C*, vol. 119, no. 8, pp. 4095–4103, Feb. 2015, doi: 10.1021/jp5116405.

[22] D. Mazzarese, A. Tripathi, W. C. Conner, K. A. Jones, L. Calderon, and D. W. Eckart, "In situ FTIR and surface analysis of the reaction of trimethylgallium and ammonia," *JEM*, vol. 18, no. 3, pp. 369–377, May 1989, doi: 10.1007/BF02657985.

[23] K. M. Bui, J.-I. Iwata, Y. Kangawa, K. Shiraishi, Y. Shigeta, and A. Oshiyama, "Reaction Pathway of Surface-Catalyzed Ammonia Decomposition and Nitrogen Incorporation in Epitaxial Growth of Gallium Nitride," *J. Phys. Chem. C*, vol. 122, no. 43, pp. 24665–24671, Nov. 2018, doi: 10.1021/acs.jpcc.8b05682.

[24] M. Kamp, M. Mayer, A. Pelzmann, and K. J. Ebeling, "On Surface Cracking of Ammonia for MBE Growth of GaN," *MRS Online Proceedings Library (OPL)*, vol. 449, ed 1996, doi: 10.1557/PROC-449-161.

[25] R. W. McCabe, "Kinetics of ammonia decomposition on nickel," *Journal of Catalysis*, vol. 79, no. 2, pp. 445–450, Feb. 1983, doi: 10.1016/0021-9517(83)90337-8.

[26] Y. Inatomi, Y. Kangawa, A. Pimpinelli, and T. L. Einstein, "Kinetic-thermodynamic model for carbon incorporation during step-flow growth of GaN by metalorganic vapor phase epitaxy," *Phys. Rev. Materials*, vol. 3, no. 1, p. 013401, Jan. 2019, doi: 10.1103/PhysRevMaterials.3.013401.

[27] S. Mita, R. Collazo, A. Rice, R. F. Dalmau, and Z. Sitar, "Influence of gallium supersaturation on the properties of GaN grown by metalorganic chemical vapor deposition," *Journal of Applied Physics*, vol. 104, no. 1, p. 013521, Jul. 2008, doi: 10.1063/1.2952027.

[28] T. Hanada, "Thermodynamic model for metalorganic vapor-phase epitaxy of N-polar group-III nitrides in step-flow growth mode: Hydrogen, competitive adsorption, and configuration entropy," *Phys. Rev. Materials*, vol. 3, no. 10, p. 103404, Oct. 2019, doi: 10.1103/PhysRevMaterials.3.103404.

[29] D. D. Koleske, A. E. Wickenden, R. L. Henry, and M. E. Twigg, "Influence of MOVPE growth conditions on carbon and silicon concentrations in GaN," *Journal of Crystal Growth*, vol. 242, no. 1, pp. 55–69, Jul. 2002, doi: 10.1016/S0022-0248(02)01348-9.

[30] X. G. He *et al.*, “Control of residual carbon concentration in GaN high electron mobility transistor and realization of high-resistance GaN grown by metal-organic chemical vapor deposition,” *Thin Solid Films*, vol. 564, pp. 135–139, Aug. 2014, doi: 10.1016/j.tsf.2014.05.045.

[31] J.-T. Chen, U. Forsberg, and E. Janzén, “Impact of residual carbon on two-dimensional electron gas properties in AlxGa1−xN/GaN heterostructure,” *Appl. Phys. Lett.*, vol. 102, no. 19, p. 193506, May 2013, doi: 10.1063/1.4804600.

Chapter 2 Control of carbon concentration with ammonia flow

The incorporation of carbon in GaN is influenced by several factors, including growth rate, pressure, temperature, and ammonia flow. The primary path for carbon to be incorporated into the film is through the gallium metalorganic. Specifically, it occurs through a mixture of trimethyl gallium, (TMGa, $Ga(CH_3)_3$), dimethyl gallium (DMGa, $Ga(CH_3)_2$), or monomethyl gallium (MMGa, $GaCH_3$). Among these species, MMGa is expected to have the highest concentration at the typical MOCVD growth temperature of approximately 1000°C[1].

To remove carbon from MMGa, the CH_3 group binds to atomic hydrogen to form CH_4, which is assumed to be non-reactive and will be swept from the system. However, since the H_2 carrier gas does not participate in any reactions, the main source of atomic hydrogen will be from NH_3 adsorbed on the growing surface. At each step of the decomposition of the NH_3, a hydrogen atom is released which can combine with a CH_3 from MMGa. Therefore, the approach will be to utilize high ammonia flows to reduce the carbon concentrations in the GaN.

Given that MMGa acts as the carbon source and ammonia provides atomic hydrogen, it is reasonable to pursue a guided empirical model that establishes a correlation between the metalorganic source (MMGa) and ammonia flow. This approach would effectively reduce the number of independent parameters required for accurate prediction of carbon incorporation. While temperature and pressure may have some influence on carbon incorporation, their primary effect involves shifting the equilibrium or activating the main process. Therefore, if it is possible to achieve the desired carbon concentrations of less than $1x10^{15}$ cm^{-3} while maintaining a constant temperature and pressure, it would simplify the process and provide greater control over carbon incorporation.

2.1 Experimental setup

All samples were grown in an Aixtron 200/4 RF-S (Aixtron SE, Herzogenrath, Germany) horizontal MOCVD reactor with the capacity for a single 2" wafer. Temperature and in-situ growth rates were determined using a LayTec epiRAS (LayTec AG, Berlin, Germany) optical measurement system. Temperature is extracted from 950 nm optical emission collected from the center of the heated SiC-coated graphite susceptor on which the substrate rests during growth. The growth rate is determined from the Fabry-Perot oscillations in 600 nm light reflected off of the

sample interfaces. All in situ growth rate measurements were done on GaN grown on sapphire because of the need for a change in the index of refraction within the sample to cause reflections. Additional growth rate information was determined using weight change or from secondary ion mass spectroscopy (SIMS) depth profiles.

With large changes in ammonia flow, total flow, and carrier gas flows, the gas dynamics can be severely disrupted. In the absence of modeling of the gas flows, the linearity of the growth rate with respect to TMGa flow is used to identify ‘good’ combinations of gas flows. The linear response should identify a condition of laminar flow of gas across the substrate and growth in a mass transport-limited regime.

Figure 2.1 illustrates the Aixtron reactor used in this work. It is a horizontal design with the input sources split into two channels, top and bottom. The metalorganics are fed through the top channel, and the hydrides through the bottom channel. To ensure minimal source mixing until reaching the hot zone, these channels are separated by a horizontal quartz plate that terminates two centimeters in front of the sample. This particular configuration effectively reduces the formation of low-temperature adducts[2]. The figure also highlights two distinct optical temperature measurement systems. The Aixtron reactor computer controls the sample heating through the bottom optical sensor, which primarily captures emissions from the lower graphite susceptor. These emissions pass through multiple quartz layers before being collected by an optical lightpipe. The upper and lower susceptors are indicated with the hatched fill in the susceptor region of the schematic. The reported sample temperatures in this study are exclusively obtained from the top susceptor, after passing through the substrates. To account for any disparities in scattering caused by the etched surfaces of the bottom substrate, a correction is applied.

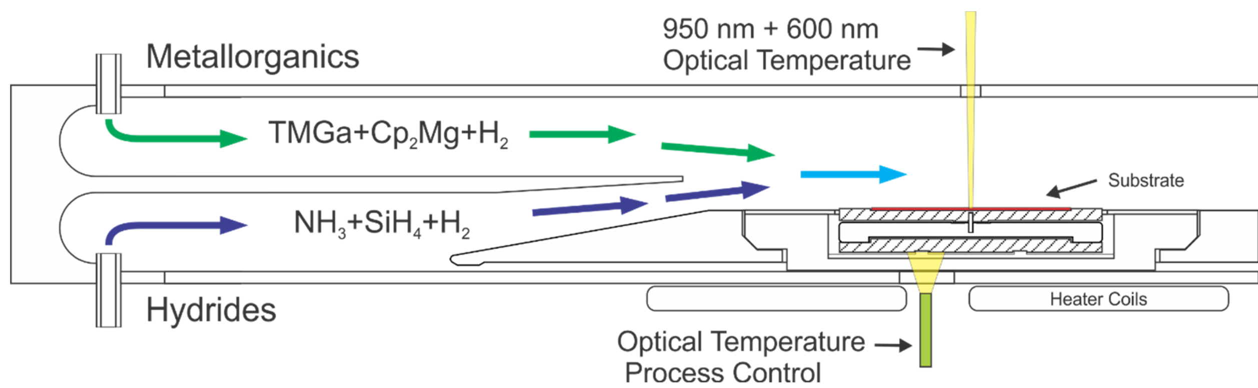

Figure 2.1 – Aixtron 200/4 RF-S growth region schematic.

Ammonia, H_2 carrier gas, and the n-type dopant silane (SiH_4) flow in the bottom hydride channel. TMGa, H_2 carrier gas, and the p-type dopant bis(cyclopentadienyl)magnesium (Cp_2Mg), flow in the top metalorganic channel. The original rationale behind the reactor design was to achieve a balanced flow of the input gas in the upper and lower channels. This produces nearly identical flows as the gas in the top and bottom channels mix, although the bottom velocity is slightly faster due to its narrower channel. This configuration ensures a smooth laminar flow throughout the substrate region. The flow conditions have been broken down into the components that make up the total flow: Total upper flow, ammonia flow, total lower flow, carrier gas to ammonia ratio in the lower hydride line, and the input flow ratio between the top and bottom flows. The breakdown of each of the flow conditions attempted is listed in Table 2.1. All gas flows are reported in either standard cubic centimeters per minute (sccm) or standard liters per minute (slm). These are flows referenced to 0°C at 1 atm, $1\ slm = 1000\ sccm$.

Table 2.1 – Reactor Flow conditions. All flow values in the table are sccm.

Growth Condition	MO Channel Flow	Hydride/MO Velocity Ratio	NH_3/H_2 Ratio	Hydride Channel Flow			Total Flow
	H_2			NH_3	H_2	Total	
Aix	**2000**	**0.98**	**1.97**	**1300**	**660**	**1960**	**3960**
A1.1	200	39.80	0.20	1300	6660	7960	8160
A1.2	200	39.80	0.49	2300	5360	7960	8160
A1.3	200	39.80	1.88	5200	2760	7960	8160
A2	**1000**	**5.36**	**0.32**	**1300**	**4060**	**5360**	**6360**
A2	**1000**	**5.36**	**32.50**	**5200**	**160**	**5360**	**6360**
A3	1895	5.36	62.50	10000	160	10160	12055
A5.3	**1300**	**6.38**	**15.60**	**7800**	**500**	**8300**	**9600**
A5.5	**1300**	**8.08**	**20.00**	**10000**	**500**	**10500**	**11800**
A6	1000	8.06	30.00	7800	260	8060	9060

2.2 Stable high ammonia growth conditions

For each flow condition, a series of layers at different TMGa flows were continuously grown. The growth rate was determined in situ by the oscillation of the reflected 600 nm light. Each data point is a sine wave fit to at least two complete oscillations, about 12 minutes of growth. Figure 2.2 shows several examples of the unstable response of the growth rate to the TMGa flow. The first three conditions, labeled A1, are very non-linear. The second two, A6 and A3, are somewhat linear

as the growth rate increases but as it decreases it does not track back the way it came. Other conditions showed a poisoning effect with a nonconstant growth rate even at a fixed TMGa flow.

The unstable flow conditions had several distinct characteristics. These include a high hydride/MO ratio (>10) resulting in turbulent mixing, and insufficient H_2 carrier in the hydride line with an NH_3/H_2 ratio greater than 20.

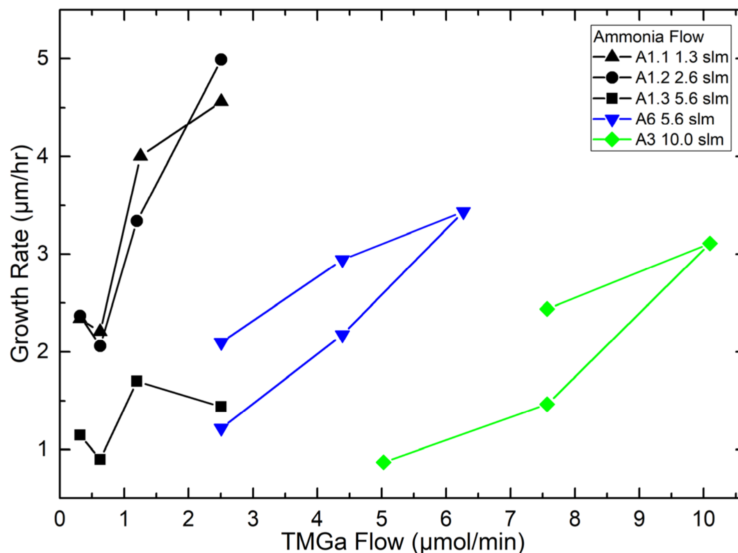

Figure 2.2 - Unstable growth rate relations. The points are connected in the order grown. The detailed gas flow conditions for each trace can be found in Table 2.1.

As indicated by bold text in Table 2.1, stable reactor flow conditions were determined for a range of ammonia flows up to 10 slm. These exhibited a linear growth rate versus TMGa flow up to 7 µm/hr and 7 µmol/min. These stable flow conditions comprised fixed H_2 carrier gas flows of 1300 and 500 sccm in the top and bottom channels, respectively, and variable ammonia flow in the bottom channel. The total flow was allowed to vary with the ammonia flow.

Figure 2.3 illustrates the linear growth rate versus TMGa flow for the conditions used in this study. The overall growth rate decreases as ammonia flow increases. Above 6 slm flow there is very little change in growth rate as ammonia flow continues to increase. The source of this reduction in the growth rate could be any stage of the growth process including gas flow, gas phase chemistry, adsorption, surface diffusion, and incorporation. With a substantial increase in ammonia flow, it might be expected that the surface coverage of nitrogen-containing molecules, NH_3, NH_2, and NH, would increase reducing access to nitrogen sites for the $GaCH_3$ molecules to adsorb on[3].

In the Aixtron reactor, TMGa is introduced from the upper channel relatively close to the hot region. As the upper and lower channels mix, it diffuses into and through the lower channel containing the ammonia. The relative mixture of gases between ammonia and hydrogen carrier

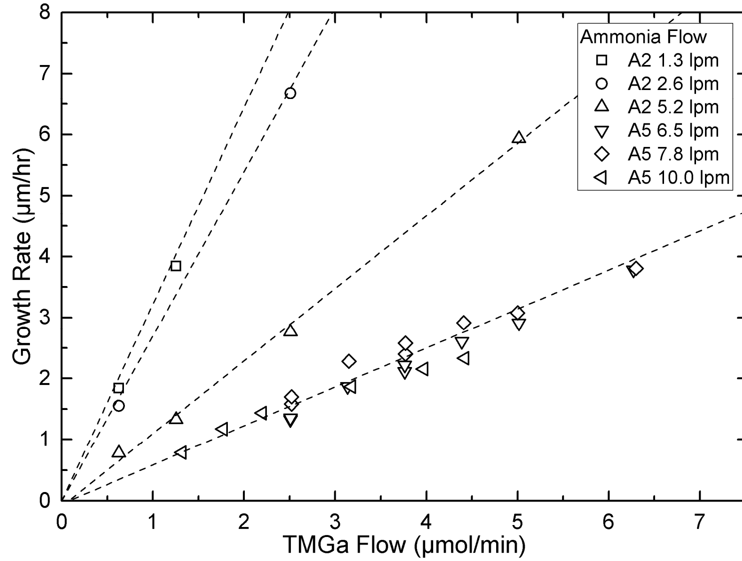

Figure 2.3 – Linear growth rate relations for reactor flow conditions used for SIMS measurements.

could affect the diffusion of the TMGa to the substrate. Binary diffusion of TMGa through either hydrogen or ammonia can be calculated with the Fuller-Schettler-Giddings equation[4].

$$D_{AB} = \frac{10^{-3} T^{1.75} \left[\frac{1}{M_A} + \frac{1}{M_B}\right]^{1/2}}{P\left[\left(\sum \nu_A\right)^{1/3} + \left(\sum \nu_B\right)^{1/3}\right]^2} \tag{2.1}$$

With $\nu_{H_2} = 7.07$, $\nu_{SF_6(TMGa)} = 69.7$, $\nu_{N_2} = 17.9, \nu_{NH_3} = 14.9$, at a pressure of 200 mbar and temperature of 1005°C, the diffusion can be calculated for TMGa in each carrier gas. $D_{TMGa\ in\ H_2} = 27.2\frac{cm^2}{s}, D_{TMGa\ in\ N_2} = 6.45\frac{cm^2}{s}, D_{TMGa\ in\ NH_3} = 8.33\frac{cm^2}{s}$. The diffusion of TMGa in ammonia is about 3 times faster than in hydrogen. The diffusion of a molecule in a mix of two different gases can be calculated with

$$D_A = \frac{1 - y_A}{\frac{y_B}{D_{AB}} - \frac{y_C}{D_{AC}}} \tag{2.2}$$

A sample was grown to evaluate diffusion through the hydride layer. Starting with the high ammonia flow condition of 10 slm, the ammonia was replaced with either H_2 or N_2 carrier gas down to 1 slm of ammonia while maintaining a constant total flow. The growth rate is plotted in Figure 2.4 against the sum of the H_2 and NH_3 flow. If the decrease in growth rate is related to the surface coverage of NH_3 and its decomposition products, swapping H_2 with N_2 without changing

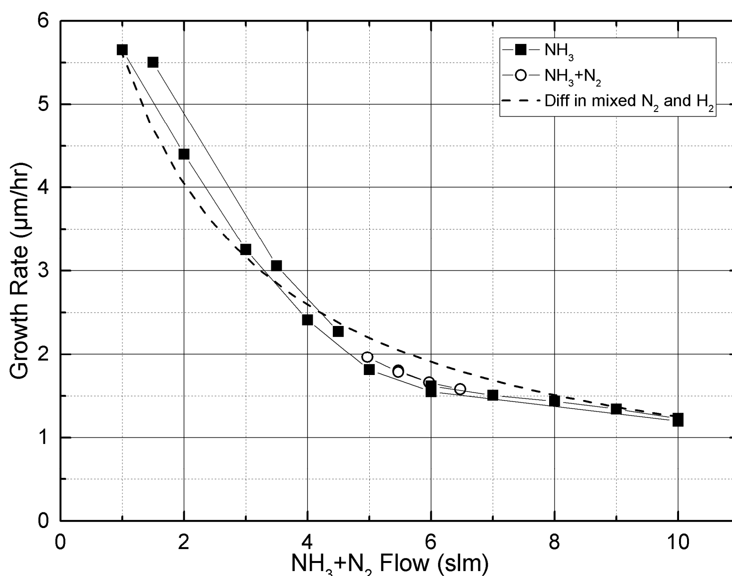

Figure 2.4 - Growth rate measured across a range of ammonia flow and carrier gas mixes. The gas mix goes from 92% hydrogen in a balance of NH_3 to 15% hydrogen. The dashed line the calculated diffusion of TMGa in a H_2/NH_3 gas mixture.

the amount of NH_3 should result in a constant growth rate. However, instead of a constant growth rate, the growth follows the curve as the sum of N_2 and NH_3. The diffusion of TMGa in N_2 and NH_3 is similar; hence, it would follow that the change in growth rate is due to the gas mixture rather than surface kinetic effects. Considering diffusion in the gas mixture, the diffusion of TMGa in a binary mixture of NH_3 and H_2 was calculated with a mixture from 15% to 95% of H_2. Seen as the dashed line in Figure 2.4, when scaled to the growth rate it correlates well with the data. The conclusion is that at least for this reactor design the gas mix in the lower hydride channel is going to impact the rate at which sources in the upper channel reach the substrate. If there is any impact

on reaction rates from changes in ammonia flow at the surface, they do not exceed the effect of the gas mixtures on diffusion.

2.3 Reducing process parameters

A series of samples were grown with several different growth rates at each ammonia flow and flow condition shown in bold in Table 2.1. Each sample was a stack of up to 10 layers at different conditions. The concentration of C, as well as Si, O, and H was measured using SIMS by EAG Laboratories. The background carbon level of the SIMS measurements was as low as $5x10^{14}$ cm^3. Minimum detection limits for Si, O, and H were $2x10^{14}$ cm^{-3}, $7x10^{14}$ cm^{-3}, and $6x10^{15}$ cm^{-3}, respectively. A representative SIMS depth profile is shown in Figure 2.5.

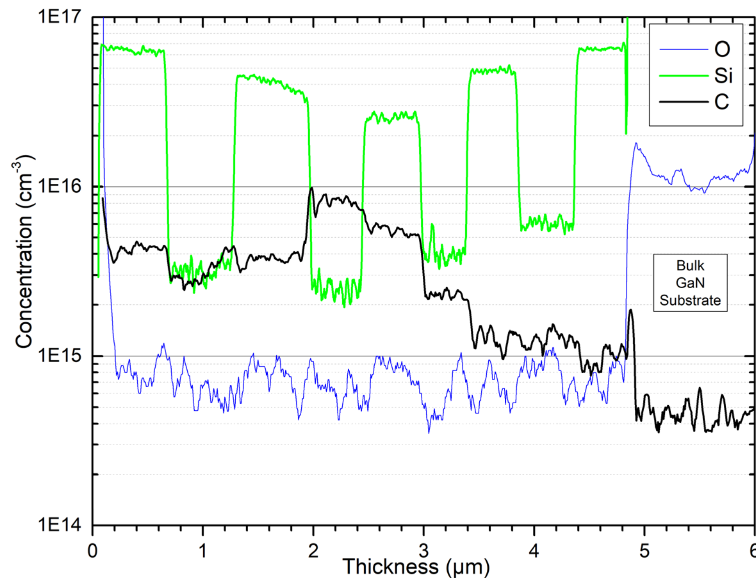

Figure 2.5 – SIMS depth profile showing O, Si, and C concentrations.

In Figure 2.6a, the carbon concentration is plotted versus the TMGa flow, revealing a linear response on the log-log plot. The concentration increases with TMGa flow and decreases with ammonia flow. This trend aligns with the observations in Figure 2.3, where an increase in ammonia flow corresponds to a decrease in the growth rate.

To isolate the effect of TMGa flow and growth rate, Figure 2.6b plots the concentration at a fixed growth rate of 1.5 μm/hr versus ammonia flow. Again, a linear response on the log-log plot is observed, which appears to be the inverse of the response to TMGa flow.

The V/III ratio is commonly evaluated in MOCVD growth due to its connections with morphology, doping, and crystal quality[5]. In this particular application, the inverse relationship between TMGa flow and ammonia flow with the carbon concentration suggests the use of the V/III ratio. Furthermore, employing the V/III ratio can help reduce the number of parameters involved.

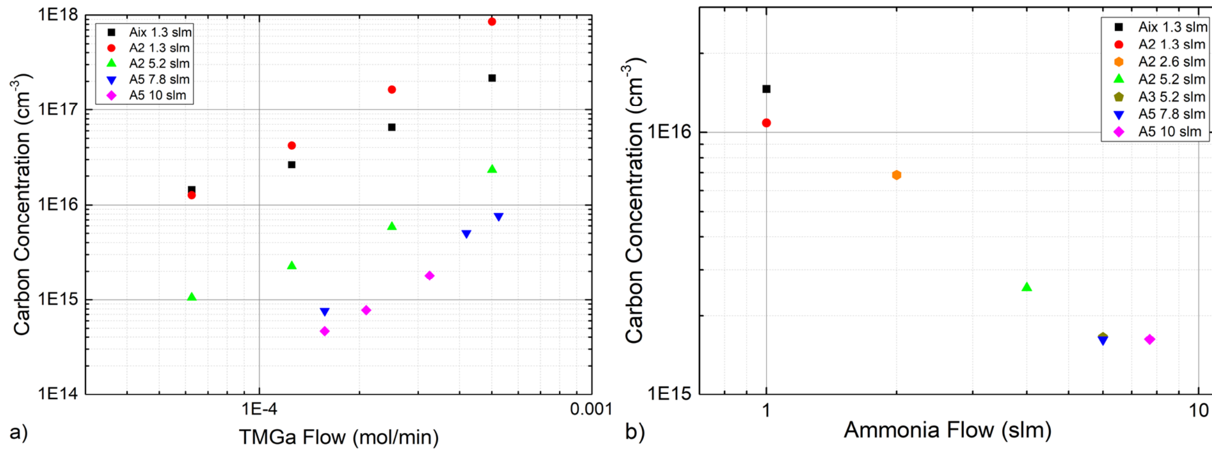

Figure 2.6 – Carbon concentration from SIMS a) versus TMGa flow, b) Versus ammonia flow with a fixed growth rate of 1.5 µm/hr and variable TMGa flow.

Plotting the carbon incorporation versus the V/III ratio in Figure 2.7a shows a promising result. The response is linear, with a fit to the data resulting in a slope of -2.0 with a residual sum of squares, the spread of the data, of 0.995. This data may be showing the impact of the decrease in growth rate with ammonia flow. However, when the carbon incorporation is plotted against the growth rate, as shown in Figure 2.7b, removing the influence of the growth rate yields a much better fit. A linear fit results in a slope of -1.3 with a residual sum of squares of 0.439, indicating a more accurate result.

In addition to ammonia flow, process conditions including temperature, pressure, and total flow can impact the growth rate relative to the TMGa flow. By utilizing the growth rate as a parameter instead of TMGa, the evaluation of the impact of the other process conditions becomes significantly simplified. The carbon incorporation rate can now be reduced to a single parameter, the ratio of ammonia flow to growth rate (V/GR). This could be considered the surface V/III ratio as long as the growth is operating in a mass transport-limited mode with no barrier between the gas and incorporation.

The relation of carbon to the V/GR ratio may indicate a specific reaction pathway for the removal of carbon during the growth process. With this simplified model, the other process variables can

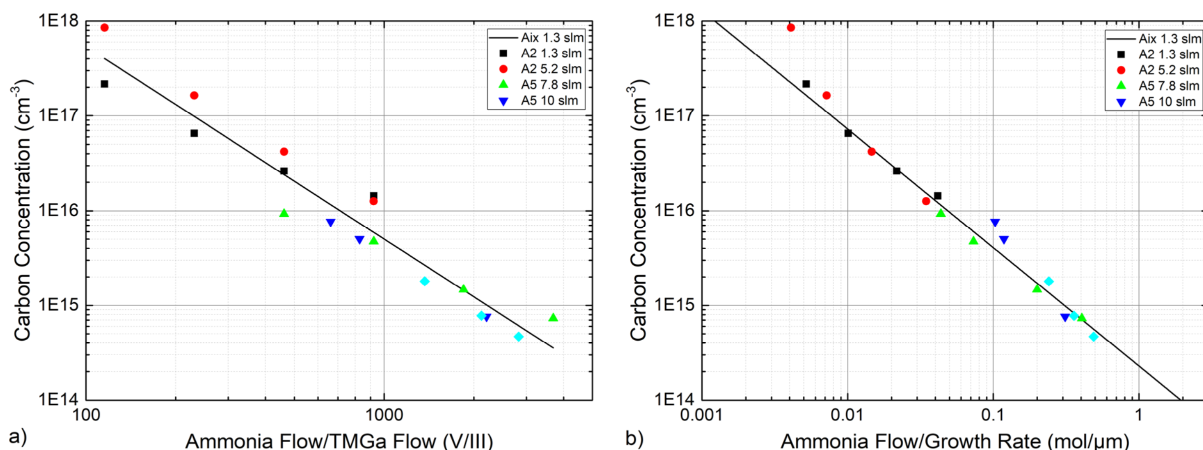

Figure 2.7 – Carbon concentration from SIMS a) versus V/III ratio, b) versus ammonia flow/growth rate.

be assessed in terms of their deviation from the empirical model fit. This approach can determine the limits or 'guardrails' within which the ammonia and growth rate can be used to control carbon incorporation.

2.4 Carbon incorporation vs temperature

A series of sample layers were grown at each of the four ammonia flows: 1.3, 5.2, 7.8, and 10 slm, at different temperatures from 950°C to 1038°C. In Figure 2.8, the carbon incorporation for each condition plotted versus V/GR.

For the lowest ammonia flow of 1.3 slm, a fixed TMGa flow of 6.27×10^{-5} mol/min was used. As the temperature increased, the growth rate decreased. However, the plot of carbon incorporation versus V/GR indicates that despite the change in growth rate, the carbon incorporation closely followed the model curve. This suggests that temperature had no impact on carbon incorporation at this growth condition, spanning a wide temperature range from 950°C to 1034°C. The temperature only affected the growth rate in this case.

At an ammonia flow of 5.2 slm, the carbon incorporation aligned with the model curve from 1020°C to 992°C. Below 992°C, it sharply increased. This behavior indicates a consistent decrease

in carbon incorporation with increasing temperature until a threshold temperature is reached, after which the carbon incorporation remains constant despite further temperature increases.

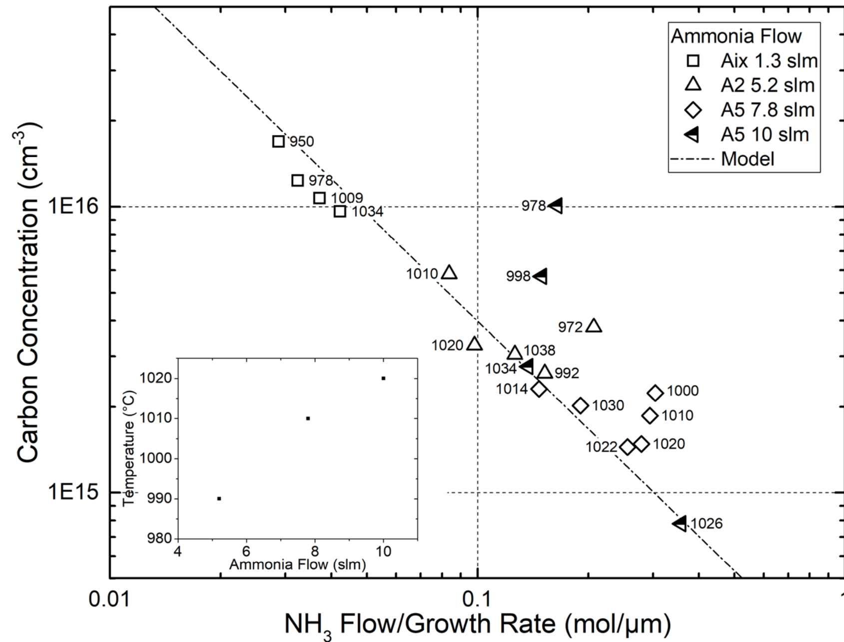

Figure 2.8 - Incorporation of carbon with respect to ammonia flow and temperature. The data point labels indicate the temperature in degrees Celsius. Inset plot shows lower temperature limit to model vs. ammonia flow.

Similarly, at an ammonia flow of 7.8 slm, the carbon incorporation tracks the model curve for the highest temperature data points. However, it deviates from the curve when the temperature drops below 1014°C. This same behavior is observed at the 10 slm condition, where temperatures below 1020°C result in a departure from the model curve. The inset in Figure 2.8 displays the minimum temperatures required to maintain the model behavior. The threshold temperature increases linearly from 990°C at an ammonia flow of 5.2 slm to 1020°C at an ammonia flow of 10 slm.

None of the existing literature has documented this specific inflection point where carbon incorporation transitions from decreasing to remaining constant with temperature[1], [6]–[8]. However, it is important to note that there is currently no available temperature response data below a carbon concentration of $1x10^{-16}$ cm^{-3}.

MOCVD growth can usually be divided into three different growth regimes: low-temperature kinetically limited, medium-temperature mass transport-limited, and high-temperature desorption limited. The mass transport-limited regime for GaN growth is from approximately 600°C at the

low temperature end to 1000 to 1050°C on the high temperature end.[9]. This would imply that most of the MOCVD growth in these experiments is in the mass transport-limited regine. While not strictly an activated process, applying the Arrhenius method to growth rate vs temperature in the mass transport-limited regime results in an apparent activation energy of 0.18 eV[10]. In the highest temperature desorption regime the process is kinetically activated with an activation energy of up to 3.5 eV[11]

To determine if there is a kinetic effect corresponding to the sharp increase of carbon at the high ammonia flow conditions, the response of growth rate to temperature was evaluated at each condition. Figure 2.9 shows two trends in the temperature response. For the lowest ammonia flow the growth is in the desorption limited regime with the growth rate decreasing with temperature. For all the higher ammonia flows, the temperature is increasing over the range of temperatures evaluated for carbon incorporation. Applying an Arrhenius analysis to the data results in apparent activation energies shown in Table 2.2. The highest ammonia flows are in the mass transport-

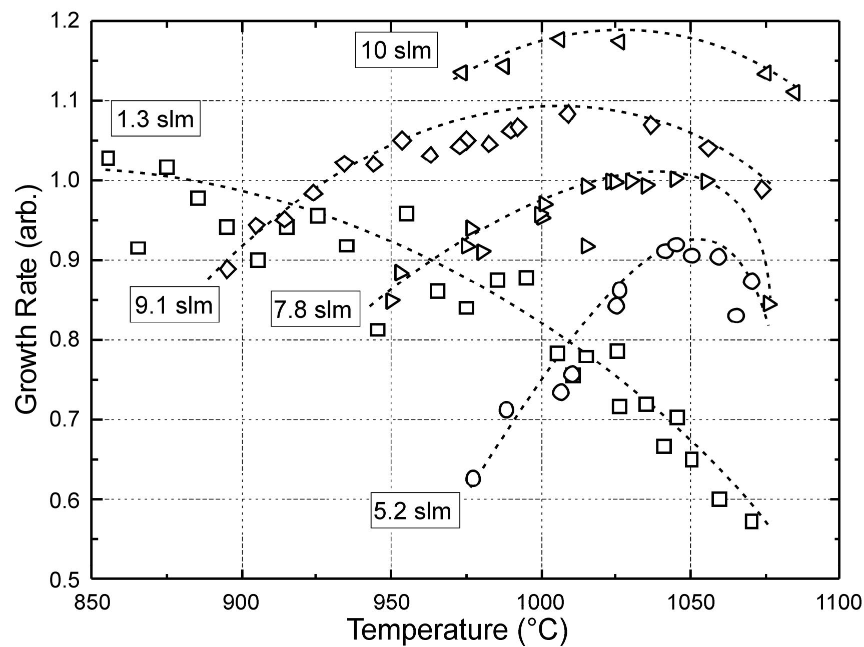

Figure 2.9 – Temperature dependence of the growth rate for ammonia flow from 1.3 – 10 slm. The data have been vertically offset for visibility. The dashed lines are drawn to guide the eye. Labels are ammonia flow.

limited regime throughout the temperature range where the carbon incorporation departs from the model. While the temperature analysis provides no insight into the carbon behavior, it does set an upper limit on usable process temperatures. It has been observed that the GaN surface transitions

from smooth to a rough ridge-like morphology as the growth enters the desorption-limited regime at ammonia flows of 5 slm or higher.

Table 2.2 – Apparent activation energies.

Ammonia Flow (slm)	E_a (eV)
5.2	0.698
7.8	0.250
9.1	0.175
10	0.182

2.5 Carbon incorporation vs growth rate

A second set of sample layers was grown at each of the four ammonia flows: 1.3, 5.2, 7.8, and 10 slm, using temperatures above the previously determined minimum values to follow the model curve. The growth rate was varied from 0.5 µm/hr to 10 µm/hr for the lowest ammonia flow and from 0.5 µm/hr to 3 µm/hr for the highest ammonia flow. When plotted against V/GR, it was observed that at lower growth rates, carbon incorporation followed the model, while at higher growth rates it deviated sharply higher than predicted by the model. This behavior aligns with the findings reported by Ciarkowski et al.[12].

To illustrate this trend, the carbon incorporation data was normalized by dividing the carbon concentration values by the value of the linear fit to all the data at that concentration. It was then plotted against the growth rate, as shown in Figure 2.10a. The graph clearly indicates that as the ammonia flow increases, the growth rate at which carbon deviates from the model decreases. For an ammonia flow of 10 slm, the maximum growth rate that conforms to the model is 1.5 µm/hr. When the ammonia flow is 10 slm, the maximum growth rate that adheres to the model is 1.5 µm/hr. At an ammonia flow of 7.8 slm, the maximum growth rate following the model slightly exceeds 2 µm/min. In contrast, at the lowest flow of 1.3 slm, the growth rate can reach 8 µm/hr before the model fails to accurately predict carbon incorporation.

The data obtained at lower ammonia flows exhibits a close alignment with the model curve across a wide range of growth rates. The maximum growth rate cutoff values are illustrated in Figure 2.10b. However, it should be noted that the data obtained at higher ammonia flows is subject to

limitations imposed by the detection limits of SIMS. As a result, the extent to which the data closely adheres to the model curve at very low growth rates becomes less certain.

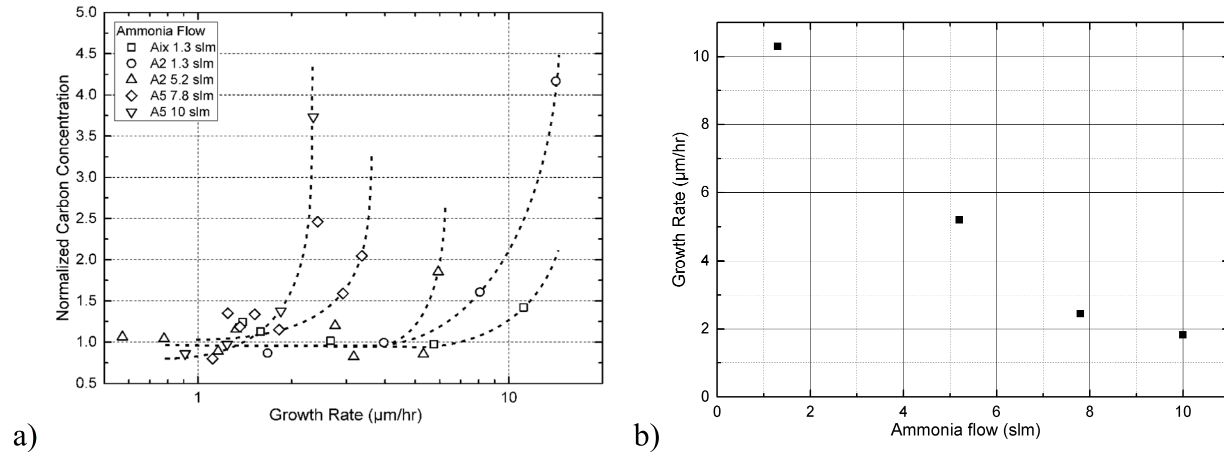

Figure 2.10 – a) Carbon concentration normalized by the model curve. The dashed lines are used as guides for the eye to see where the data departs from the model curve. b) Maximum growth rate cutoff values.

2.6 Conclusion

If all of the available carbon incorporation data that is both above the minimum temperature limit for each ammonia flow and below the maximum growth rate limit is plotted against V/GR, the plot in Figure 2.11 results. A linear fit to this data results in a slope of -1.25 with the residual sum of squares of 0.329 and an r-square, the goodness of fit, of 0.979. Within these bounds this could represent a constant reaction pathway over the entire range of carbon incorporation from 2×10^{14} cm^{-3} to 1×10^{17} cm^{-3}

If this were considered in the form of a reaction rate equation it could be written

$$r = k[A]^m[B]^n \tag{2.3}$$

$$carbon\ concentration = k(NH_3\ flow)^{-1.25}(growth\ rate)^{1.25} \tag{2.4}$$

With $k = 2.34 \times 10^{14}$ and a reaction order for ammonia of -1.25, and for the growth rate of 1.25. Fractional reaction order is not surprising when considering the numerous intermediate reactions involved in the growth process.

It is noteworthy that carbon incorporation can be effectively represented by a simple ratio. However, if we were to consider the ammonia flow and growth rate as independent variables, a

multiple regression fit could be performed to explore their combined effect. The results of this fit are presented in Table 2.3

Table 2.3 – Carbon incorporation fit data.

Fit	k	NH_3	GR	Residual Sum of Squares	R-Square
Single	2.34×10^{14}	-1.25	1.25	0.33	0.98
Multiple	2.78×10^{14}	-1.12	1.37	1.79	0.98

The fit assuming equal and opposite reaction orders for ammonia flow and growth rate cannot be improved upon. This would indicate the ratio of the V and III components is crucial, rather than considering the nitrogen or gallium source independently.

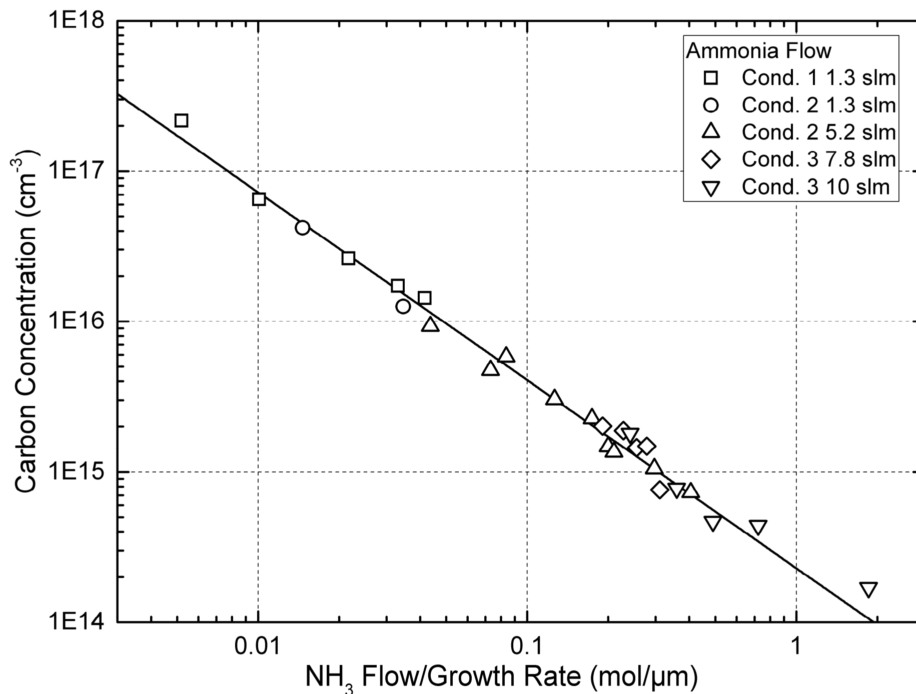

Figure 2.11 – Carbon concentration for all ammonia flows with temperature and growth rate limits applied.

The dependence of carbon incorporation on V/GR is not unexpected. Figure 2.12 depicts the carbon incorporation data from the literature, which has been replotted in relation to V/GR. Similar trends to this work are found although mostly at higher carbon levels. It is important to note that these trends were derived from different reactors and varying growth conditions. Table 2.4

provides an overview of the reactor configurations used in the referenced data. Each of these curves can be considered characteristic of their respective reactors.

Among the reference studies, the reactor configuration used by Piao et al.[13] bears the closest resemblance to the Aixtron 400RF utilized in this work. Piao reported experiments conducted at Taiyo Nippon Sanso using a TNSC SR4000 reactor. The behavior of these curves defines an endpoint for this kind of manipulation. Notably, it is worth mentioning that achieving such behavior necessitates significant amounts of ammonia and increasing temperatures, which are subject to a strict upper limit due to the potential degradation of morphology.

Table 2.4 – Reactor styles in references.

Reference	Reactor style	Wall material	Hot/Cold Wall
Danielsson[1]	Horizontal	SiC coated graphite	Hot
Koleske[6]	Close Coupled Showerhead	Stainless	Cold
Kaess[14]	Vertical	Quartz	Cold
Piao[13]	Horizontal	Quartz	Cold

It was found that the unintentional carbon incorporation in GaN grown via MOCVD could be accurately described with a single parameter consisting of the ratio of ammonia flow to growth rate. This behavior is constrained by two factors: a maximum growth rate that decreases with increasing ammonia flow, and a minimum temperature that decreases as ammonia flow increases. By operating within the bounds of this guided empirical model, precise control over unintentional carbon incorporation can be achieved, ranging from $1x10^{17}$ to $5x10^{14}$ cm^{-3}, while allowing independent adjustment of growth rate. This demonstrates the potential for achieving desirable electrical properties in devices through effective control of unintentional carbon incorporation during MOCVD growth of GaN.

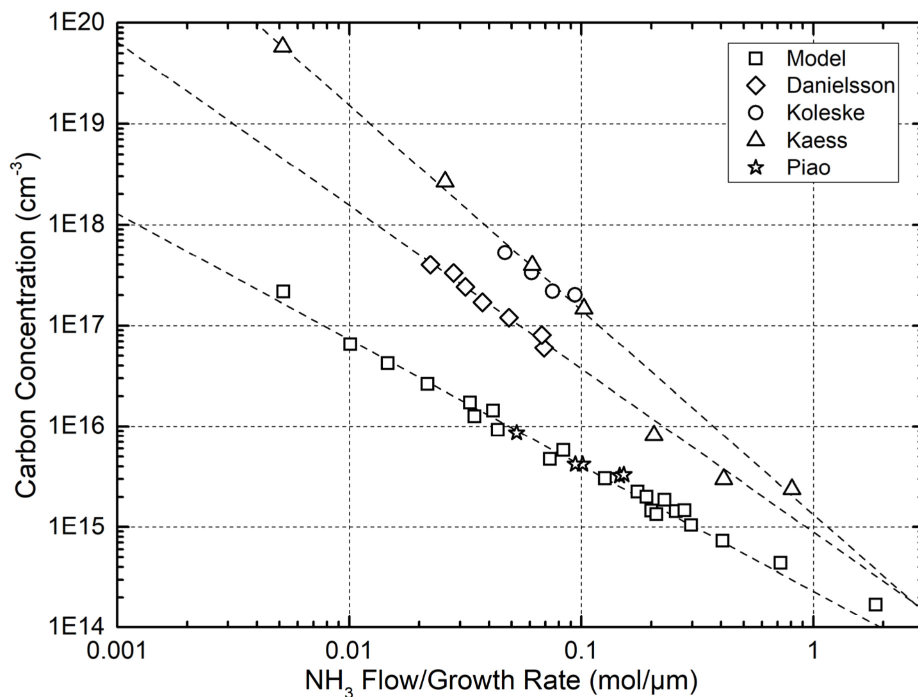

Figure 2.12 – Data from this work compared to previous works with carbon incorporation replotted versus V/GR. The data is from Danielsson[1], Koleske[6], Piao[13], and Kaess[14].

References

[1] Ö. Danielsson, X. Li, L. Ojamäe, E. Janzén, H. Pedersen, and U. Forsberg, "A model for carbon incorporation from trimethyl gallium in chemical vapor deposition of gallium nitride," *J. Mater. Chem. C*, vol. 4, no. 4, pp. 863–871, Jan. 2016, doi: 10.1039/C5TC03989D.

[2] H. Hardtdegen *et al.*, "On the influence of gas inlet configuration with respect to homogeneity in a horizontal single wafer MOVPE reactor," *Journal of Crystal Growth*, vol. 223, no. 1–2, pp. 15–20, Feb. 2001, doi: 10.1016/S0022-0248(00)00969-6.

[3] K. M. Bui, J.-I. Iwata, Y. Kangawa, K. Shiraishi, Y. Shigeta, and A. Oshiyama, "Reaction Pathway of Surface-Catalyzed Ammonia Decomposition and Nitrogen Incorporation in Epitaxial Growth of Gallium Nitride," *J. Phys. Chem. C*, vol. 122, no. 43, pp. 24665–24671, Nov. 2018, doi: 10.1021/acs.jpcc.8b05682.

[4] E. N. Fuller, P. D. Schettler, and J. Calvin. Giddings, "NEW METHOD FOR PREDICTION OF BINARY GAS-PHASE DIFFUSION COEFFICIENTS," *Ind. Eng. Chem.*, vol. 58, no. 5, pp. 18–27, May 1966, doi: 10.1021/ie50677a007.

[5] D. D. Koleske, A. E. Wickenden, R. L. Henry, W. J. DeSisto, and R. J. Gorman, "Growth model for GaN with comparison to structural, optical, and electrical properties," *Journal of Applied Physics*, vol. 84, no. 4, pp. 1998–2010, Aug. 1998, doi: 10.1063/1.368353.

[6] D. D. Koleske, A. E. Wickenden, R. L. Henry, and M. E. Twigg, "Influence of MOVPE growth conditions on carbon and silicon concentrations in GaN," *Journal of Crystal Growth*, vol. 242, no. 1, pp. 55–69, Jul. 2002, doi: 10.1016/S0022-0248(02)01348-9.

[7] X. G. He *et al.*, "Control of residual carbon concentration in GaN high electron mobility transistor and realization of high-resistance GaN grown by metal-organic chemical vapor deposition," *Thin Solid Films*, vol. 564, pp. 135–139, Aug. 2014, doi: 10.1016/j.tsf.2014.05.045.

[8] J.-T. Chen, U. Forsberg, and E. Janzén, "Impact of residual carbon on two-dimensional electron gas properties in AlxGa1−xN/GaN heterostructure," *Appl. Phys. Lett.*, vol. 102, no. 19, p. 193506, May 2013, doi: 10.1063/1.4804600.

[9] T. Mihopoulos, "Reaction and transport processes in OMCVD : selective and group III-nitride growth," Thesis, Massachusetts Institute of Technology, 1999. Accessed: Mar. 19, 2023. [Online]. Available: https://dspace.mit.edu/handle/1721.1/9655

[10] N. Kaluza, R. Steins, H. Hardtdegen, and H. Lueth, "MOVPE GaN growth: determination of activation energy using in-situ reflectometry," *Journal of Crystal Growth*, vol. 272, no. 1–4, pp. 100–105, Dec. 2004, doi: 10.1016/j.jcrysgro.2004.08.060.

[11] D. D. Koleske, A. E. Wickenden, R. L. Henry, J. C. Culbertson, and M. E. Twigg, "GaN decomposition in H2 and N2 at MOVPE temperatures and pressures," *Journal of Crystal Growth*, vol. 223, no. 4, pp. 466–483, Mar. 2001, doi: 10.1016/S0022-0248(01)00617-0.

[12] T. Ciarkowski *et al.*, "Connection between Carbon Incorporation and Growth Rate for GaN Epitaxial Layers Prepared by OMVPE," *Materials*, vol. 12, no. 15, p. 2455, Jan. 2019, doi: 10.3390/ma12152455.

[13] G. Piao *et al.*, "Study of carbon concentration in GaN grown by metalorganic chemical vapor deposition," *Journal of Crystal Growth*, vol. 456, pp. 137–139, Dec. 2016, doi: 10.1016/j.jcrysgro.2016.08.030.

[14] F. Kaess *et al.*, "Correlation between mobility collapse and carbon impurities in Si-doped GaN grown by low pressure metalorganic chemical vapor deposition," *Journal of Applied Physics*, vol. 120, no. 10, p. 105701, Sep. 2016, doi: 10.1063/1.4962017.

Chapter 3 Additional extrinsic dopants and compensators

To achieve minimally compensated n-GaN suitable for use for high voltage p-n diodes (5 kV or higher), it is crucial to identify all dopants with concentrations equal to or exceeding $1x10^{15}$ cm^{-3}. Extrinsic dopants can be relatively easily identified by utilizing SIMS to survey all atoms other than Ga or N. However, it is important to note that not all extrinsic atoms will be electrically active, and their presence may have minimal impact on the electron concentration in the drift layer.

Several dopants commonly found in MOCVD-grown GaN, such as iron, magnesium, oxygen, and silicon, are of particular concern. Each of these dopants has unique sources, and their reduction may require thorough investigative work to determine if changes in handling procedures, materials, or growth conditions can effectively mitigate their presence. Identifying and addressing the sources of these dopants is crucial for achieving the desired electrical characteristics in n-GaN for high-voltage diode applications.

3.1 Silicon

The dominant dopants that come from the MOCVD source materials are carbon and silicon. Carbon incorporation has been modeled as a function of V/GR. A similar procedure can be done for silicon. Silicon is an intentional dopant (ID). It is supplied by silane gas that enters the reactor in the lower flow channel, along with the ammonia. Silicon is also an unintentional dopant (UID). With no silane flowing into the reactor silicon will still be found incorporated into the GaN film. During the development of the carbon model, silicon incorporation was measured simultaneously. For each TMGa flow and ammonia flow, a silicon data point was acquired with no silane flowing, representing the UID silicon, and one with silane flowing, representing a combination of UID and ID silicon. Figure 3.1 shows a typical SIMS sample for a multilayered sample with two silicon concentrations for each growth rate. The intentional silicon concentration is determined by subtracting the concentration with silane flowing from the concentration with no silane flowing.

Because Si competes for Ga sites, it is predicted that the incorporation should be inversely proportional to the Ga incorporation, and therefore to the growth rate. This holds for both intentional and unintentional silicon. Since silane and ammonia are mixed in the lower flow channel before it enters the reactor, it is reasonable to assume that at a fixed growth rate, silicon incorporation should be proportional to silane flow. Silicon incorporation was measured in a series

of samples with growth rates ranging from 1-10 µm/hr and ammonia flow rates of 1.3 to 10 slm. Figure 3.2 illustrates the intentional silicon incorporation with respect to silane flow/GR. This results in a linear relation on the log-log plot with a reaction order of one. The ammonia flow has no impact on the silicon incorporation up to 10 slm.

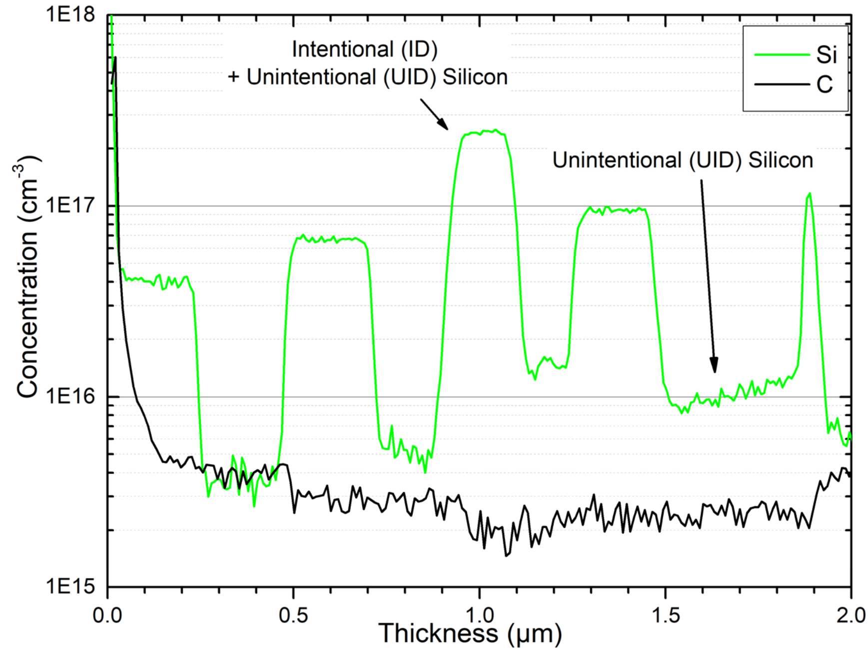

Figure 3.1 – SIMS data at a fixed ammonia flow of 10 slm.

This reactor as well as many others has unintentional sources of Si. The most common source suggested is the hot quartz hardware. The SiC-coated graphite susceptor has also been considered. For this reactor, there are two locations where the quartz gets hot enough to accumulate GaN. There is a quartz ring surrounding the susceptor that, based on GaN accumulation, is quite hot. The source gases flow directly over it before reaching the substrate. Over many growth and cleaning cycles, the quartz will become eroded. In addition, the inside of the quartz liner above the substrate is heated by the hot gas surrounding the susceptor and can also accumulate GaN. Either of these could act as a fixed source of silicon.

The behavior of unintentional silicon incorporation, without the presence of silane flow, differs significantly from intentional silicon incorporation. Figure 3.3 shows the UID silicon incorporation extracted from the SIMS. As the growth conditions shift towards higher ammonia flows, there is a notable decrease in silicon incorporation. However, once an ammonia flow of 7.8 slm is reached, there is no further reduction and silicon concentrations. The silicon concentrations for the 7.8 and

10 slm ammonia flows are indistinguishable and fall within the same range. In comparison to intentional silicon incorporation, the response to changes in growth rate is weaker, especially at lower ammonia flows. Each grouping represents a fixed source of silane at different flow rates. The decrease in silicon incorporation exhibits a roughly linear correlation with the decrease in growth rate when TMGa is held constant and ammonia flow is increased. This observation

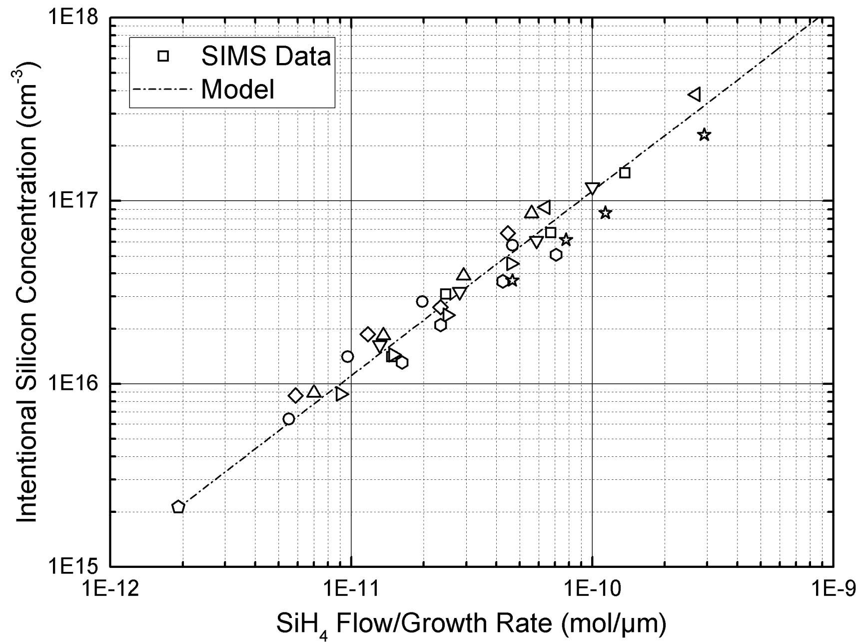

Figure 3.2 – Intentional silicon concentration.

suggests that the fixed source of silicon is located inside of the liner above the susceptor. As the gas composition transitions from predominantly hydrogen to primarily ammonia, silicon experiences a reduction in the diffusion rate similar to that observed for TMGa.

Carbon, unintentional Si, and intentional Si can now be predicted and controlled using ammonia flow, Silane flow, and growth rate. When growing on sapphire, the growth rate can be determined during the growth via reflectometry. When growing on GaN, the growth rate relations documented during the development of the carbon incorporation model will be used.

3.2 Unintentional Fe doping

Iron is another potential source of compensation in MOCVD GaN. First-principles calculations have indicated that it is incorporated into GaN at gallium sites and behaves as an acceptor-like state with the energy of $E_C - 0.5\ eV$[1]. DLTS measurements have correlated a trap at this energy

with Fe concentrations[2]. It is often used to create insulating layers[3], [4] and has also been identified as an unintentional contaminant in the MOCVD growth of GaN[5].

The initial development of low carbon GaN involved the use of GaN substrates that were diced into 1 cm squares. This approach was adopted to maximize the utilization of substrates that were initially scarce. The diced substrates were coated with a protective photoresist layer and then subjected to dicing using a diamond saw. Following the dicing process, the chips underwent a cleaning procedure involving solvents and acid treatment, typically piranha etch or Aqua Regia. Subsequently, they were rinsed with deionized water (DI).

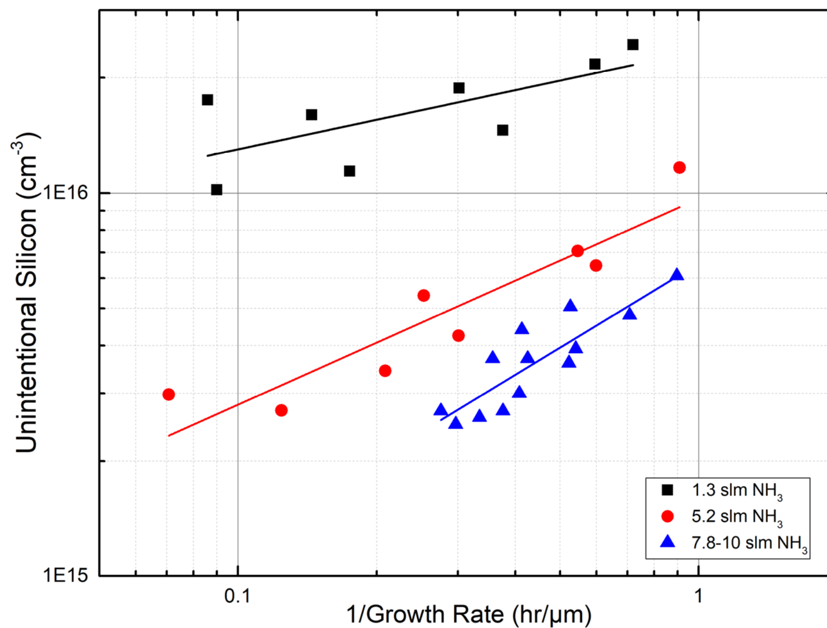

Figure 3.3 – Unintentional silicon incorporation. Legend is ammonia flow.

However, it was observed that many of these samples exhibited unexpectedly low electron concentrations. To investigate this issue, it was hypothesized that metal contamination might be the cause. Subsequently, the chips were analyzed using SIMS, revealing the presence of elevated concentrations of Fe, Mg, and Al, reaching levels as high as $1x10^{18}$ cm^{-3}.

Several experiments were designed to evaluate conditions under which the GaN becomes contaminated with Fe and whether growth conditions can reduce the Fe contamination. The first experiment was designed to determine whether Fe contamination resulted from the cleaning and handling of the samples.

Table 3.1 describes the chemicals and cleaning procedures utilized. All chemicals used are Baker Analyzed® Electronic Grade.

Table 3.1 – Wafer Cleaning Procedures.

Type	Procedure	Time	Temperature
Deionized (DI) water - 18 MΩ-cm from Elga Purelab Ultra Purifier	Rinse under flowing DI water. Blow off with dry N_2.	10 min	Room Temp
Solvent – Acetone CMOS electronic Grade	First Rinse under flowing Acetone to waste to remove the majority of photoresist. Soak in sonicator	5 min	Room Temp
Solvent – Methanol Semi Grade	Rinse acetone into waste with flowing Methanol. Soak in sonicator	5 min	Room Temp
Piranha Etch – 4:1 H_2SO_4 :30% H_2O_2 Electronic grade	Soak	10 min	100°C
Aqua Regia – 3:1 $HCl:HNO_3$	Soak	10 min	Allow to naturally heat up. Close to 100°C

A series of successive growths were performed on the same GaN on sapphire template. SIMS was then used to determine the concentration of Fe, Al, and Mg for each layer. Table 3.2 details the experiment steps.

Table 3.2 – Steps in the handling/cleaning experiment.

Step	Cleaning	Configuration	Fe Behavior
1	None	Full bare epi-ready sapphire wafer	$4x10^{15}$ cm^{-3} constant
2	Rinse with 18 MΩ-cm DI water, blow dry with N_2	Full wafer	$4x10^{15}$ cm^{-3} decreasing to $2x10^{15}$ cm^{-3}
3	Soak in 100°C Piranha etch, rinse with 18 MΩ-cm DI water, blow dry with N_2	Full wafer	$6x10^{15}$ cm^{-3} decreasing to $5x10^{15}$ cm^{-3}
4	Coat with S1813 photoresist (PR) and hard bake, remove PR with solvents, soak in 100°C Piranha etch, rinse with 18 MΩ-cm DI water, blow dry with N_2	Full wafer	$1.7x10^{16}$ cm^{-3} decreasing to $3x10^{16}$ cm^{-3}

5	Coat with S1813 photoresist (PR) and hard bake, dice wafer into five pieces with a center 1cm square, remove PR with solvents, soak in 100°C Piranha etch, rinse with 18 MΩ-cm DI water, blow dry with N_2	Diced into 5 pieces with 1 cm center square	3×10^{15} cm^{-3} increasing to 3×10^{16} cm^{-3}
6	Soak center 1 cm chip in aqua regia, rinse with 18 MΩ-cm DI water, blow dry with N_2	Diced into 5 pieces with 1 cm center square	3×10^{16} cm^{-3} increasing to 6×10^{16} cm^{-3}

The SIMS data of the first experiment is shown in Figure 3.4.

The conclusions from this experiment are:

1) Regrowth and DI water do not add additional Fe to subsequent growths. This can be seen with the drop in the Fe concentration in step 2.
2) Acids, solvents, and PR add some additional Fe contamination, but at these temperatures, it decreases as the growth proceeds. This can be seen in steps 3 and 4.
3) Coating with PR and dicing the wafer did not add any additional metal contamination. This is indicated by the lack of a significant spike in Fe at the beginning of step 5.
4) Growing with a diced wafer showed evidence of an additional significant source of iron contamination that increased steadily as the growth proceeded.
5) The impact of Aqua Regia is inconclusive because it appears to be swamped by Fe coming from the susceptor.

The second experiment was an evaluation of the temperature response of the metal contamination. A GaN wafer was diced by hand with a diamond scribe and rinsed in DI water. An epi-ready sapphire wafer was also diced by hand into four pieces with a one-centimeter piece removed from the center. There is a recess in the susceptor in which the substrate sits. This recess is about 1 mm larger than the substrate. When the pieces are assembled there can be up to 1 mm gaps between the pieces. This is the minimum amount of handling to get a multi-piece substrate into the reactor to evaluate the impact of exposed areas of the susceptor near the center. Four 1 µm layers were grown at temperatures of 970, 100, 1030, and 1055°C.

The four layers are indicated in Figure 3.5a. The concentration of the metal contaminants was very high, over 1×10^{17} cm^{-3} for three of the layers. This would indicate that exposed regions of the

susceptor may be contaminating the films. There is a very clear temperature response with contamination decreasing at 1000°C and below and increasing above 1000°C.

The final measurement of metal contamination was conducted under the most stringent conditions. A single full GaN wafer, which had been cleaned by the manufacturer, was carefully opened and installed in the reactor within an inert gas environment. During the measurement process, three layers of GaN were grown on the wafer.

After the initial layer of 9 µm of GaN was grown, the wafer was removed from the reactor and measured on a Hg probe. To facilitate the measurement, the wafer was positioned with its top surface facing down contacting the plastic platen of the Hg probe.

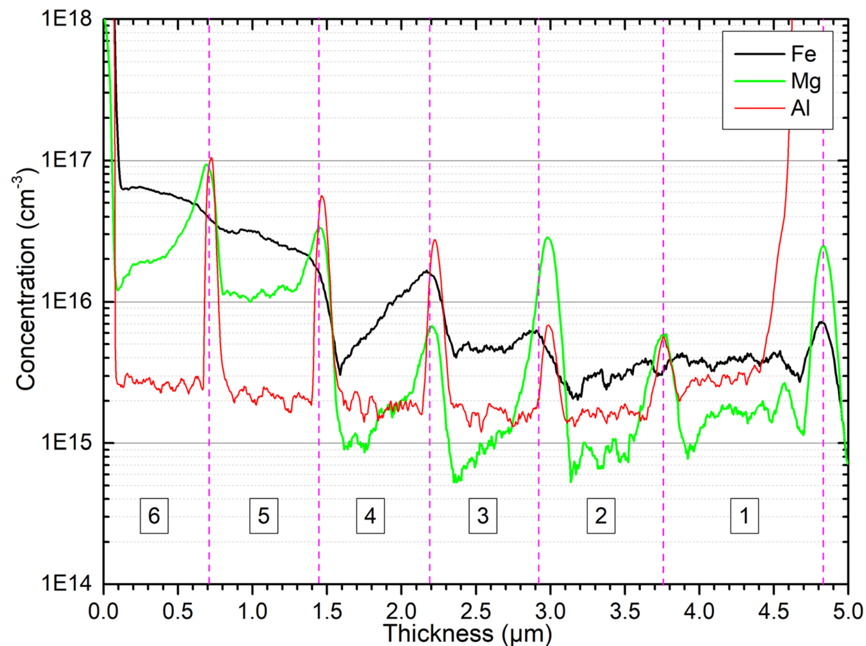

Figure 3.4 – SIMS analysis for metal contamination. Experiment steps are labeled at bottom.

Subsequently, the wafer underwent a cleaning process involving piranha etch, followed by rinsing with deionized (DI) water. Following the cleaning step, an additional two microns of GaN were grown on the wafer. The wafer was once again removed from the reactor, its weight was measured, and it was subsequently returned to the reactor for the final growth step involving an additional 2 µm of GaN.

Figure 3.5b shows the SIMS data for the Fe, Mg, and Al concentrations. They are all at the detection limit. The Fe concentration was no more than $7x10^{14}$ cm^{-3}. While there is a spike in each

of the metal concentrations after the wafer was removed and measured, it quickly dropped close to the level of the thick layer. This is very different from the behavior of Fe in the diced wafer which continued to increase at similar temperatures.

When the susceptor is occupied with an uncut substrate, the Fe levels are low enough to have only minimal effect on the electron concentrations. The reason for the spikes observed at the growth interfaces is still unknown, but they decrease rapidly enough that they are not anticipated to have any significant impact during thick growth processes. Additionally, Al and Mg are also detected. Although their levels can be relatively high under certain conditions, they are consistently lower than the Fe levels. Unless electron concentrations of less than $1x10^{15}$ cm^{-3} are targeted, it is not necessary to account for these dopants in the growth process when using complete wafers. The presence of these dopants is expected to have minimal impact on the doping levels and overall properties of the GaN layers. Therefore, their consideration becomes relevant only when aiming for extremely low electron concentrations.

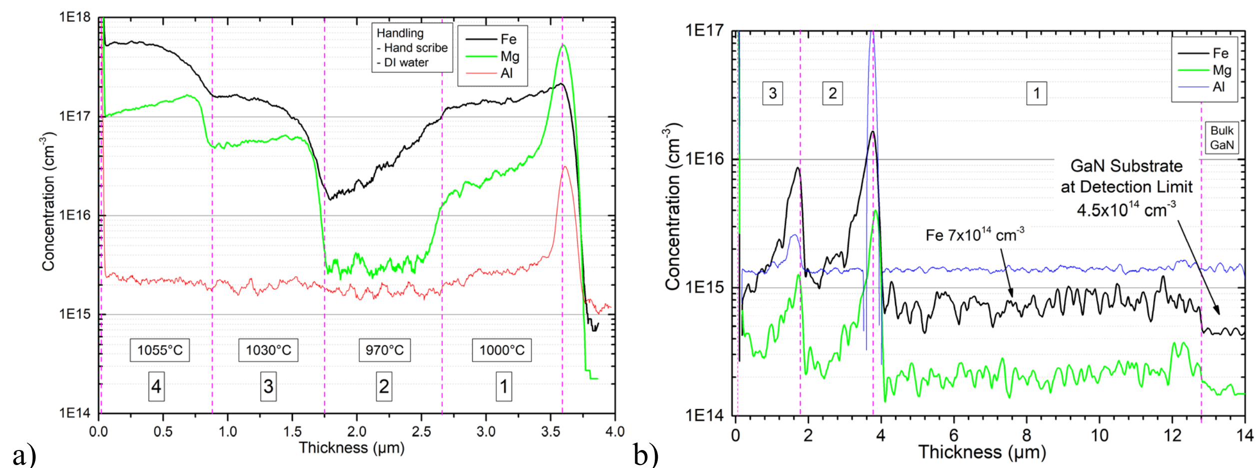

Figure 3.5 – SIMS analysis for metal contamination. a) temperature response b) Growth of thick GaN layer on HVPE GaN full wafer.

3.3 Unintentional oxygen doping

Unintentional oxygen contamination has been a recurring problem in the MOCVD growth of GaN films and is a major contributor to n-type conduction in undoped GaN films. Oxygen has a low formation energy, replacing nitrogen atoms in the lattice[6]. It is a shallow donor of 27 meV below the conduction band[7] that readily ionizes providing conduction electrons. The sources of oxygen

may include reactor contamination from exposure to air, reactor material outgassing, growth sources[8], and carrier gases.

The oxygen concentration in the grown films was collected along with all SIMS measurements of silicon and carbon. Figure 3.6 shows a typical SIMS measurement of a thick GaN sample. The oxygen concentration is measured as 6.66×10^{14} cm^{-3}. This is right at the detection limit of the SIMS measurement. All other samples consistently show oxygen concentrations at the SIMS detection limit. Unintentional oxygen does not appear to contribute appreciably to the conduction electrons in our samples. This is likely due to the purity of currently available metalorganic and hydride sources and rigorous efforts to minimize reactor exposure to air. All samples are introduced into the reactor through a nitrogen-purged glovebox. The reactor is continuously purged with clean nitrogen 24 hours a day and air exposure has been avoided for more than a year.

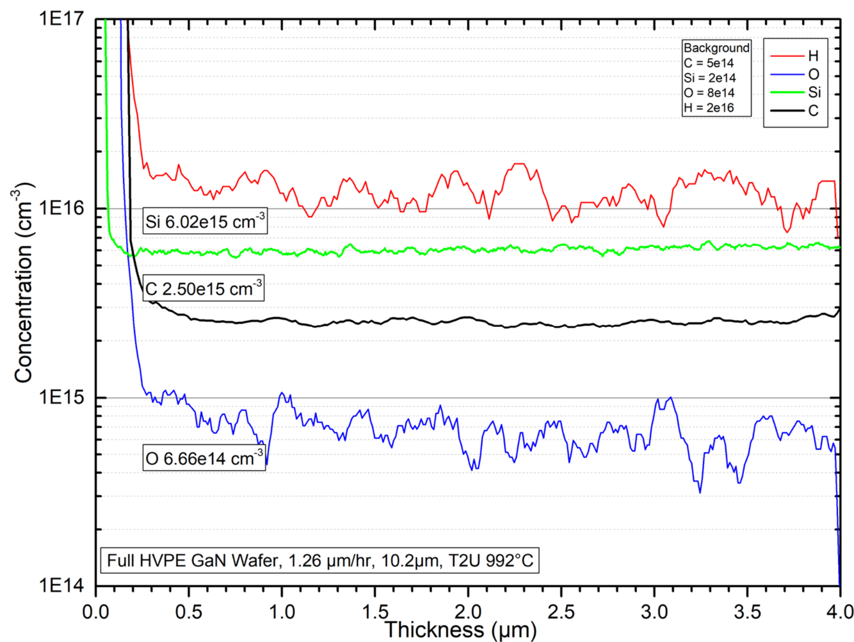

Figure 3.6 – SIMS measurement of C, Si, O, and H for a 10 µm thick sample grown on a full SCIOCS GaN wafer.

3.4 Intentional Mg doping

Magnesium, in addition to being an unintentional dopant in the growth of n-GaN, is used to create p-type conditions in GaN. The intentional Mg source used is bis(cyclopentadienyl)magnesium (Cp_2Mg) which is introduced into the reactor in the top metalorganic flow channel. Magnesium is

expected to be proportional to the Cp_2Mg flow. But, because it incorporates on a gallium site, like silicon, the incorporation should be proportional to the inverse of the growth rate. Figure 3.7 shows Mg concentration determined by SIMS for several different Cp_2Mg flows and growth rates as well as two different ammonia flows. For a fixed ammonia flow the incorporation does occur as expected. Mimicking the behavior of Ga incorporation from TMGa, because it is introduced in the top channel, the incorporation decreases with increased ammonia flow due to a decreased diffusion

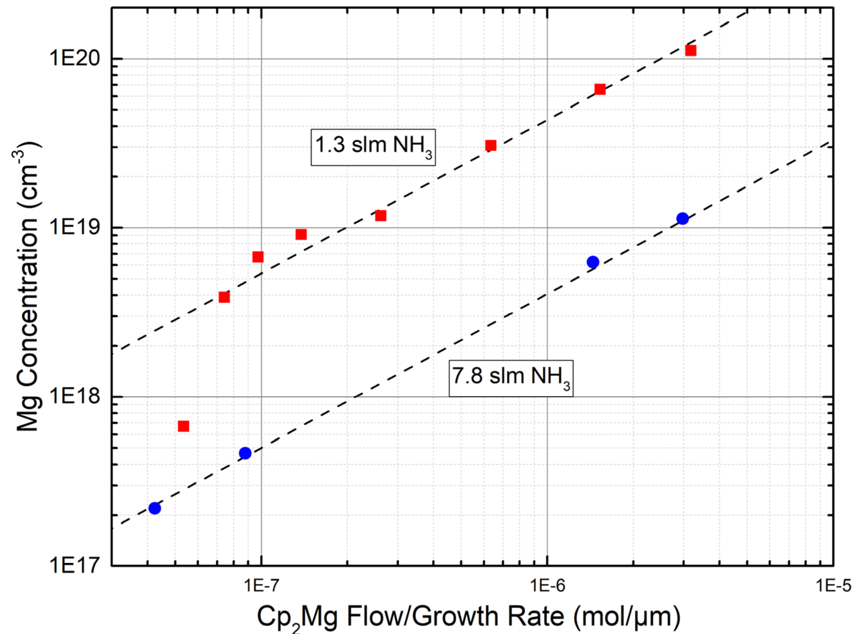

Figure 3.7 – Magnesium incorporation at 1.3 and 7.8 slm ammonia flow.

rate. This does limit the maximum Mg doping concentration, which is needed for very highly doped contact layers, at high ammonia flows. To avoid disturbing the interface at the p-n junction, the initial layer of p-GaN must be grown at the same high ammonia flows as the drift layer. However, once the p-GaN is growing, the growth conditions can transition to low ammonia flows to achieve the highest Mg doping for the surface contact layer.

3.5 Conclusions

Several extrinsic dopants, including carbon, were investigated, and, in addition to those, intentional dopants such as silicon and magnesium were also studied. The concentration of intentional dopants, silicon, and magnesium, can be modeled using a simple linear fit based on their respective source flows and growth rates. When utilizing full wafers in the reactor, the only

remaining extrinsic dopant that has an impact on electron concentration is unintentional silicon. Although the relationship for unintentional silicon is not as straightforward as that of intentional silicon, it is still possible to determine its concentration at various fixed ammonia flows and for growth rates ranging from 1 to 10 μm/hr.

References

[1] Y. S. Puzyrev, R. D. Schrimpf, D. M. Fleetwood, and S. T. Pantelides, “Role of Fe impurity complexes in the degradation of GaN/AlGaN high-electron-mobility transistors,” *Appl. Phys. Lett.*, vol. 106, no. 5, p. 053505, Feb. 2015, doi: 10.1063/1.4907675.

[2] M. Horita, T. Narita, T. Kachi, and J. Suda, “Identification of origin of EC –0.6 eV electron trap level by correlation with iron concentration in n-type GaN grown on GaN freestanding substrate by metalorganic vapor phase epitaxy,” *Appl. Phys. Express*, vol. 13, no. 7, p. 071007, Jun. 2020, doi: 10.35848/1882-0786/ab9e7c.

[3] A. Y. Polyakov, N. B. Smirnov, A. V. Govorkov, and S. J. Pearton, “Electrical and optical properties of Fe-doped semi-insulating GaN templates,” *Applied Physics Letters*, vol. 83, no. 16, pp. 3314–3316, 2003, doi: 10.1063/1.1621458.

[4] A. Y. Polyakov, N. B. Smirnov, A. V. Govorkov, and S. J. Pearton, “Properties of Fe-doped semi-insulating GaN structures,” *Journal of Vacuum Science and Technology B: Microelectronics and Nanometer Structures*, vol. 22, no. 1, pp. 120–125, 2004, doi: 10.1116/1.1633776.

[5] Y. Zhang *et al.*, “Probing unintentional Fe impurity incorporation in MOCVD homoepitaxy GaN: Toward GaN vertical power devices,” *Journal of Applied Physics*, vol. 127, no. 21, p. 215707, Jun. 2020, doi: 10.1063/5.0008758.

[6] C. G. Van de Walle, C. Stampfl, and J. Neugebauer, “Theory of doping and defects in III–V nitrides,” *Journal of Crystal Growth*, vol. 189–190, pp. 505–510, Jun. 1998, doi: 10.1016/S0022-0248(98)00340-6.

[7] R. Y. Korotkov and B. W. Wessels, “Electrical Properties of Oxygen Doped GaN Grown by Metalorganic Vapor Phase Epitaxy,” *MRS Internet Journal of Nitride Semiconductor Research*, vol. 5, no. 1, pp. 301–307, Dec. 2000, doi: 10.1557/S1092578300004427.

[8] M. A. di Forte-Poisson *et al.*, “Relationship between physical properties and gas purification in GaN grown by metalorganic vapor phase epitaxy,” *Journal of Crystal Growth*, vol. 195, no. 1, pp. 314–318, Dec. 1998, doi: 10.1016/S0022-0248(98)00584-3.

Chapter 4 Electronic properties

The models of extrinsic dopant incorporation can now be applied to determine electron conduction in GaN. Within the concentration range of $1x10^{15}$-$1x10^{17}$, all extrinsic dopants have either been reduced to below $1x10^{15}$ or modeled based on the growth conditions. This model enables the specification of growth conditions that yield a particular electron concentration with a specific compensation ratio possible with the reactor configuration. Deviations from the predicted behavior can identify intrinsic compensators that are difficult to measure directly.

4.1 Using the model

Figure 4.1 presents the model calculation at four ammonia flows: 1.3, 5.2, 7.8, and 10 slm. The plot depicts the expected carbon incorporation (Na) with black squares, the UID and ID silicon

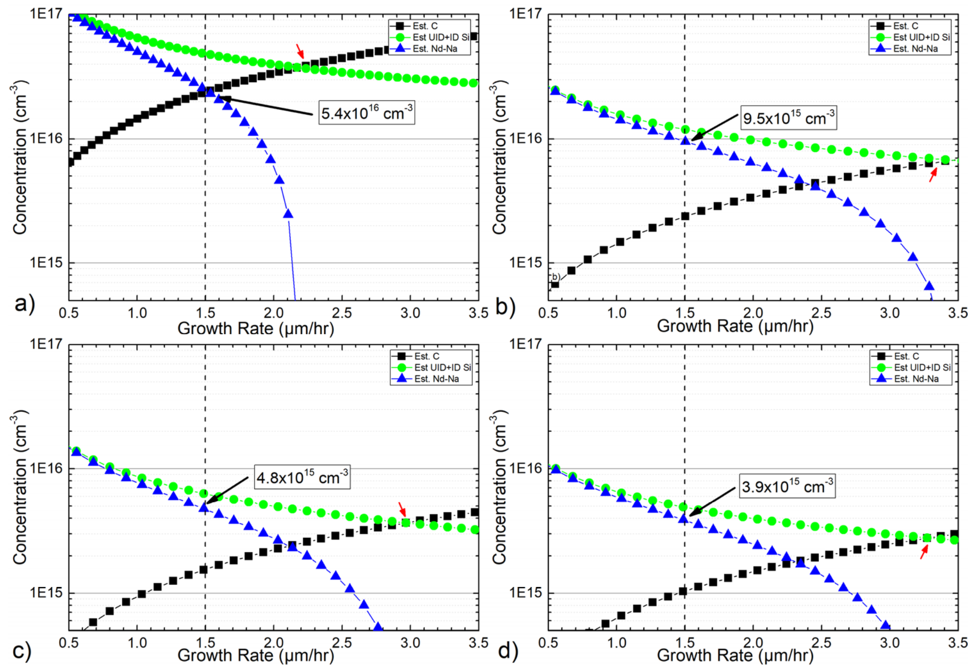

Figure 4.1 – Plot of the model to choose growth conditions for the desired electron concentration. Ammonia flow a) 1.3 slm, b) 5.2 slm, c) 7.8 slm, d) 10 slm.

incorporation (Nd) with green circles, and the difference between Nd and Na with blue triangles. According to the exclusion of other dominant extrinsic dopants determined in the previous chapter, the difference Nd-Na is expected to correspond to the electron concentration.

To achieve the desired electron concentration and compensation ratio, a suitable growth rate is selected considering the trade-off between silicon incorporation decrease and carbon incorporation increase at higher growth rates. In this specific example, a growth rate of 1.5 µm/hr and a silane flow are chosen to achieve a compensation ratio of approximately 20% for each ammonia flow. The expected electron concentrations at these conditions are indicated at the intersections of the dashed line for each ammonia flow in Figure 4.1.

The plot provides practical guidelines for selecting electron concentrations. It should be noted that the model predictions may have an error of up to $\pm 2x10^{15}$ cm^{-3}. As the concentrations of carbon and silicon approach each other, the slope of the curve representing the electron concentration becomes steep, resulting in increased variability and the potential for having more compensators than donors. This scenario leads to a fully depleted, insulating material. The red arrows in Figure 4.1 indicate the growth rate at which a fully depleted film would occur for each ammonia flow.

4.2 Experiment

The electrical test samples are grown either on GaN templates or bulk GaN substrates. A template is a layer of GaN grown on a sapphire substrate using the two-step method[1]. This consists of growing a low-temperature GaN nucleation layer on the wafer, annealing it, and then adding 1 µm GaN at the typical high growth temperature of 1030°C. For growth on GaN substrates, the reactor temperature is brought to 800 ° C with hydrogen carrier gas and ammonia flowing. It is kept at this temperature for 5 min to drive off any volatiles on the surface but avoid decomposition of the GaN itself. The test layers are the same for both GaN substrates and templates and consist of a 250 nm n+GaN layer followed by 2-10 µm of n-GaN.

The electron concentration is measured using an MDC mapping Hg Probe. An HP 4192A impedance analyzer is used to measure the capacitance-voltage (CV) characteristic from which the electron concentration is extracted.

4.3 Heteroepitaxial growth on GaN templates

The first set of electrical test samples was grown on sapphire templates at conditions known to produce conductive n-type films. For each ammonia flow rate, individual samples were grown with decreasing silane flows until films could no longer be produced with n-type conductance. Hg probe CV measurements were taken on the samples, and the electron concentration at zero bias

was reported. Figure 4.2 shows a parity plot comparing the estimated electron concentrations (represented by filled squares) with the measured electron concentrations. The lowest estimated electron concentration that showed n-type conductance was 7×10^{15} cm^{-3}. Any attempt at growing samples with lower concentrations resulted in fully depleted films. The arrow in the figure indicates samples grown with an estimated electron concentration of 3×10^{15} cm^{-3} that were fully depleted. This behavior suggests that there are additional sources of intrinsic compensation that

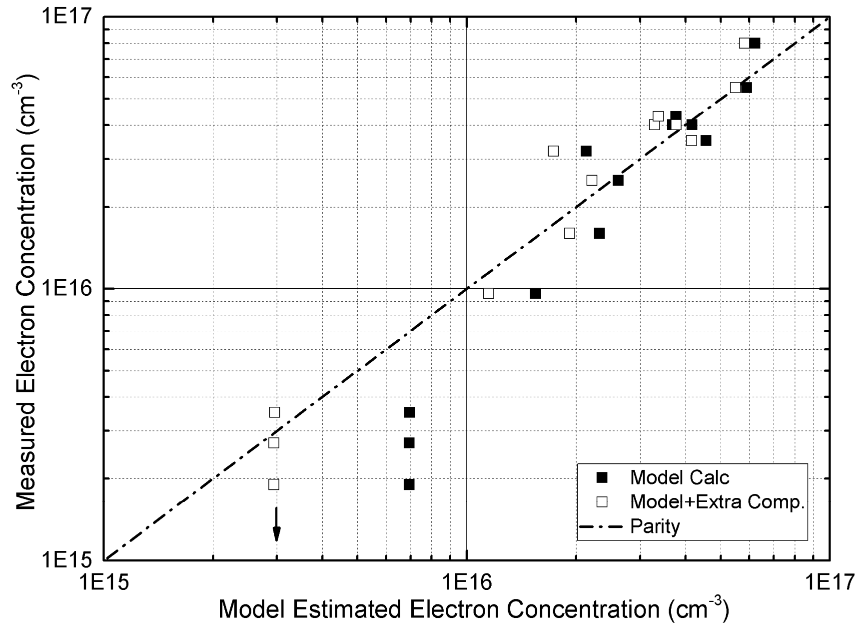

Figure 4.2 – Parity plot of carbon incorporation in GaN on sapphire. The solid points are raw model estimates of electron concentrations, and the hollow points are the estimate with an additional 4×10^{15} cm^{-3} of compensation added.

have not been accounted for. The estimated electron concentration with an additional 4×10^{15} cm^{-3} of intrinsic compensation added is shown in the figure as hollow squares, which come much closer to parity.

GaN grown on sapphire with MOCVD typically has a dislocation density of 10^8 to 10^{10} cm^{-2}[2], [3] . These dislocations can act as a source of compensation. Neugebauer and Van de Walle suggest that Ga vacancies will spread along the dislocation as a row of closely space acceptor centers that can compensate electrons.[4] Kyle et al. used mobility measurements to estimate a dislocation-related trap density for GaN on sapphire.[5] The trap density ranged from 3×10^{15} cm^{-3} with a dislocation density of ~5×10^8 to 6×10^{16} cm^{-3} with a dislocation density of 5×10^9 cm^{-3}. The estimate

of an unknown compensator in the GaN on sapphire films grown here is consistent with dislocations as the source.

4.4 Homoepitaxial growth on HVPE GaN

The next set of samples was grown on HVPE GaN substrates supplied by SCIOCS (Sumitomo Electric). The targeted range of electron concentrations was from 1x10^{16} cm^{-3} down to 1x10^{15} cm^{-3}. Samples were grown with decreasing silane flows until films with n-type conductance could no longer be produced. Hg probe CV measurements were taken on the samples, and the electron concentration at zero bias was reported. Figure 4.3 shows a parity plot comparing the estimated electron concentrations (represented by filled squares) with the measured electron concentrations. The lowest possible predicted electron concentration to show n-type conduction is 3.5x10^{15} cm^{-3}. Any value lower than this results in a fully depleted film. The arrow in the figure indicates samples grown with an estimated electron concentration of 1.8x10^{15} cm^{-3} that were fully depleted. The estimated electron concentrations consistently read higher than those measured. If an additional fixed 2.2x10^{15} cm^{-3} compensation is added to the model, the model prediction matches the measured electron concentrations.

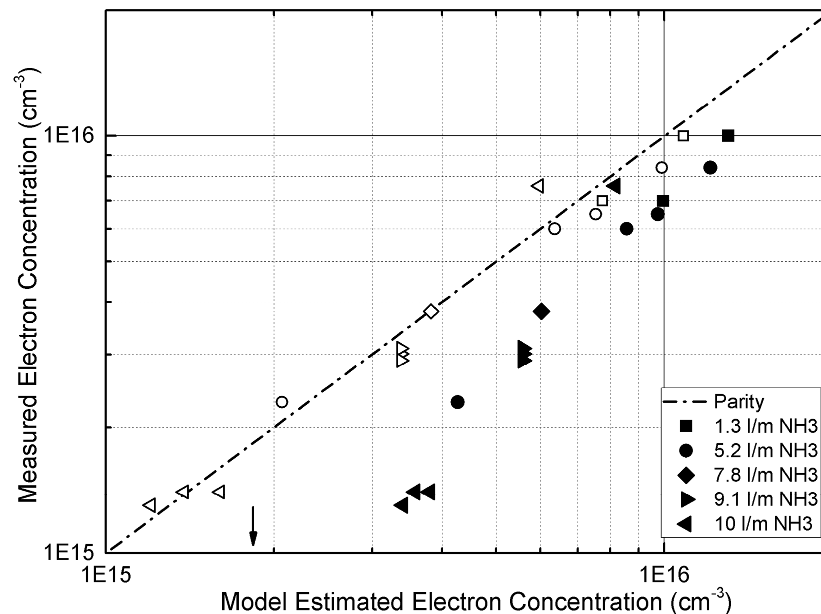

Figure 4.3 – Parity plot for samples growth on HVPE GaN substrates. The solid points are raw model estimates of electron concentrations, and the hollow points are the estimate with an additional 2.2x10^{15} cm^{-3} of compensation added.

The source of compensation identified for samples grown on sapphire, dislocations, is not expected to be significant in growth on GaN substrates. The dislocation density measured by the manufacturer of the substrates averages $2x10^6$ cm^{-2}. Kyle et al.[5] found that for GaN with a dislocation density in this range the dislocation-related trap concentration was $1.7x10^{14}$ cm^{-3}. Although dislocations may not be the source of compensation in these samples, several intrinsic point defects that have been observed in GaN films could be the source of this compensation. For instance, A trap located at E_C- 0.6 eV has been identified[6] associated with a nitrogen anti-site defect, N_{Ga}[7], [8], however Van de Walle[9] claims it is unlikely with an unfavorable formation energy. Others have measured concentrations of gallium vacancies as high as $1x10^{19}$ cm^{-3}, especially at high V/III ratios[10]–[12] however these tend to be associated with oxygen impurities that are very low in these samples.

Adding the unknown intrinsic compensator, the model plots have been recalculated in Figure 4.4. A horizontal asymptote at $2.2x10^{15}$ cm^{-3} can be now seen in the black Na line.

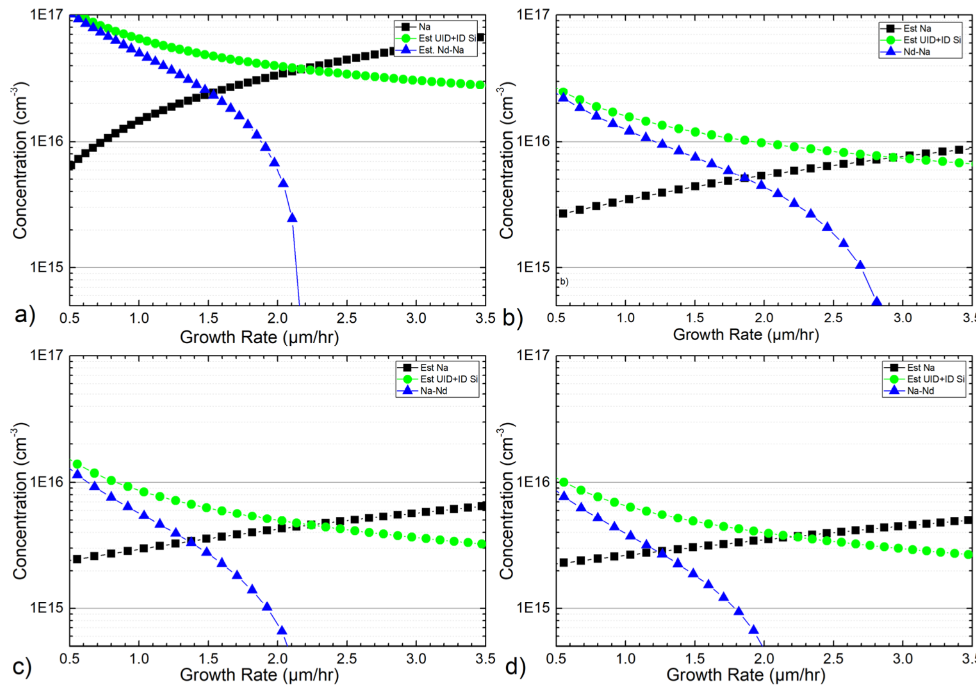

Figure 4.4 – Plot of adjusted model to use to choose growth conditions for the desired electron concentration with 50% compensation. Ammonia flow a) 1.3 slm, b) 5.2 slm, c) 7.8 slm, d) 10 slm.

Upon discovering an additional compensation source with a concentration of 2.2×10^{15} cm^{-3}, the model calculations were revised for accurate electron concentration prediction for device growth. The inclusion of these additional compensators leads to an increase of approximately 30-40% in the compensation ratio, diminishing the advantages of the low carbon incorporation at the highest ammonia flows.

As the compensation ratio rises, the sensitivity of the electron concentration to minor variations in the growth process intensifies, both across the wafer and throughout the film's thickness. This effect becomes evident when examining the electron concentration measurements across the width of the depletion layer. In a typical capacitance-voltage (CV) plot, the trace begins at the depletion depth under zero bias conditions. By applying an increasing reverse bias voltage, the depletion width expands and the plot outlines the electron concentration in the newly depleted regions. This process continues until the depletion width exceeds the layer thickness, a reverse breakdown occurs, or the voltage limit of the measuring instrument is reached.

Figure 4.5a illustrates the electron concentration of a sample grown with an ammonia flow of 7.8 slm and a SiH_4 flow of 7.13×10^{-13} mol/min. The model calculation results in a compensation ratio of 90%. However, the electron concentration exhibits oscillations as the depletion width increases, indicating a less-than-ideal behavior. In contrast, Figure 4.5b displays measurements from samples grown at all four ammonia flows, showcasing relatively stable electron concentrations with

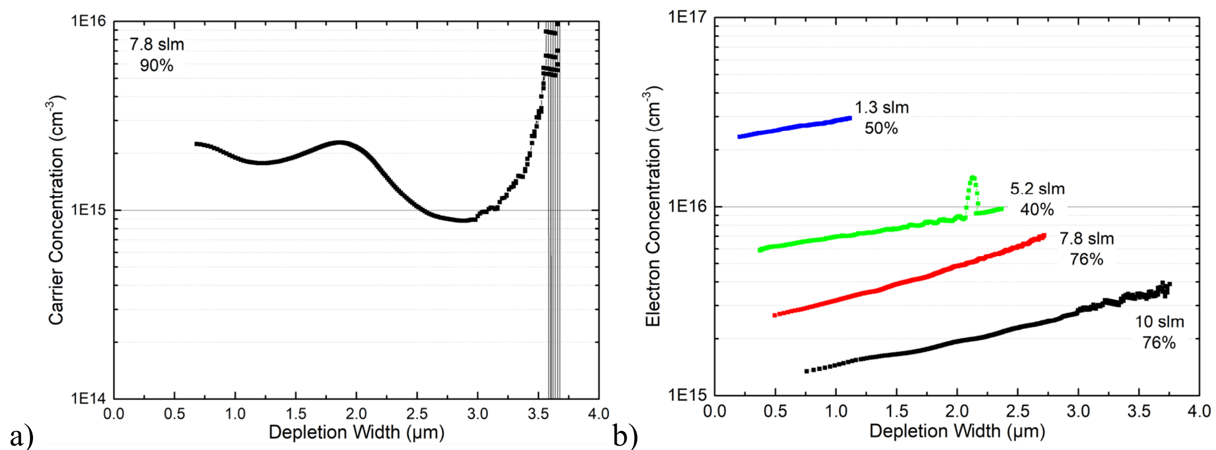

Figure 4.5 – Electron concentrations extracted from Hg Probe C-V. GaN on GaN homoepitaxy. a) uneven electron concentration at 90% compensation, b) good electron concentration profile at a maximum of 76% compensation.

compensation ratios of up to 76%. Despite the additional 2.2×10^{15} cm^{-3} in compensating dopants, the resulting electrical properties still demonstrate satisfactory quality.

4.5 p-n Diode Growth

Using the revised model, the complete p-n device with the structure shown in Figure 4.6a was grown. The drift layer doping is designed to reach up to 5 kV before reverse breakdown. Figure 4.6b displays the reverse characteristic measurement of a fully fabricated device, where the breakdown voltage was measured to be 3.15 kV. It is worth noting that the device breakdown occurred specifically at the edge of the p-GaN contact. However, it should be acknowledged that the design of the p-GaN profile has not been optimized to fully leverage the potential of the n-GaN drift layer. The doping and electron concentration of the drift layer for this device were calculated using the model inputs outlined in

Table 4.1.

Table 4.1 – Model calculations for 5kV n-GaN drift layer.

NH3 Flow	NH3 Flow	TMGa Flow	GR	Thick	NH_3/ GR	SiH_4 Flow	SiH_4 Flow/GR	ID Si	UID Si	UID+ID Si	Carbon	Unknown Comp	Nd-Na	Cmp Ratio
sccm	mol/min	mol/min	µm/hr	µm		mol/min		cm^{-3}	cm^{-3}	cm^{-3}	cm^{-3}	cm^{-3}	cm^{-3}	
10000	0.446	2.1×10^{4}	1.20	29.5	0.372	2.3×10^{12}	1.92×10^{12}	2.4×10^{15}	4.0×10^{15}	6.4×10^{15}	8.710^{14}	2.2×10^{15}	3.3×10^{15}	0.48

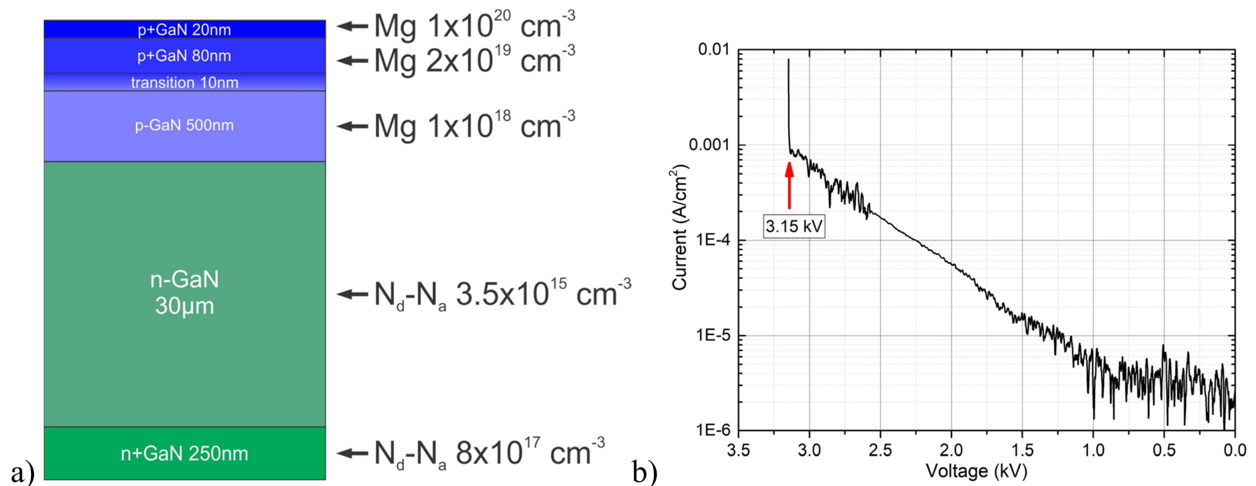

Figure 4.6 – a) p-n device structure schematic and b) measured reverse breakdown voltage of fabricated device.

This sample was grown under conservative conditions, specifically using a low growth rate of 1.2 µm/hr. This approach was chosen to achieve a low compensation ratio. The growth process took approximately 25 hours to complete. If higher compensation ratios are acceptable, and the target is an electron concentration of $3x10^{15}$ cm^{-3} with a compensation ratio of 70%, a higher growth rate of 3.5 µm/hr could be employed. This would enable the production of a similar p-n diode within a shorter timeframe of 10 hours. A model plot illustrating these conditions is depicted in Figure 4.7 using a SiH_4 flow of $2.2x10^{-11}$ mol/min

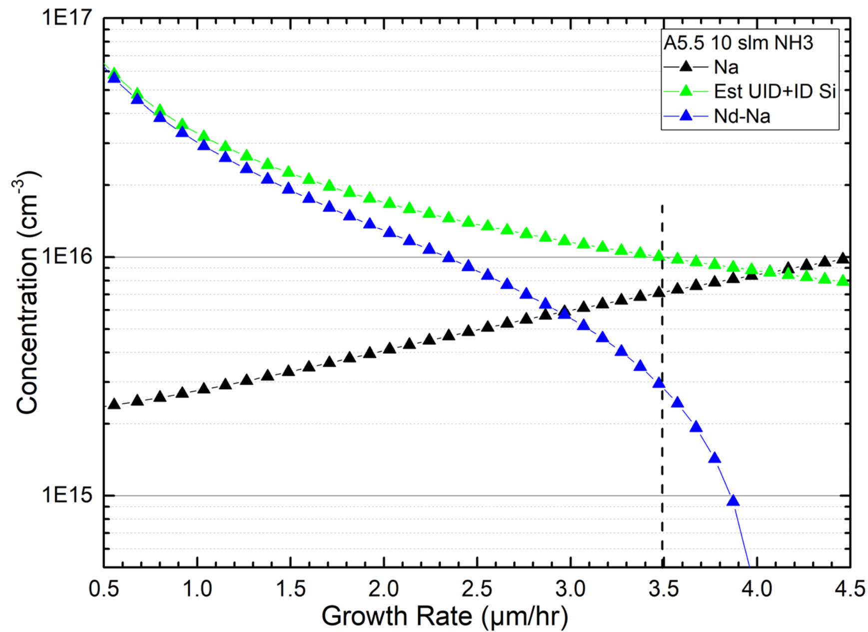

Figure 4.7 – Model calculation for maximum growth rate.

4.6 Conclusions

An empirical model was developed to accurately predict the major extrinsic dopants in the MOCVD growth of GaN-based on specific growth conditions. At the highest ammonia flow and a growth rate of 1.5µm/hr, this model predicts a minimum electron concentration of $1x10^{15}$ cm^{-3} with a compensation ratio of 20%. However, when incorporating precise estimates of extrinsic dopants from the empirical model, it was discovered that an unknown intrinsic dopant exists with a concentration of $2.2x10^{15}$ cm^{-3} in growth on HVPE GaN substrates. Unfortunately, without a means to mitigate this defect, it reduces the ultimate electrical properties initially anticipated based on the model.

Nevertheless, under similar growth conditions, it is feasible to reliably produce a drift layer with an electron concentration of 2.5×10^{15} cm^{-3} and a compensation ratio of 60%. Full p-n diodes were successfully grown with drift layers of 30 µm and an electron concentration of 3×10^{15} cm^{-3}. These diode structures possess the potential for a reverse breakdown voltage greater than 5 kV. The highest measured breakdown achieved thus far from these diode structures is 3.2 kV.

References

[1] S. Nakamura, "GaN growth using GaN buffer layer," *Jpn. J. Appl. Phys*, vol. 30, pp. L1705–L1707, 1991.

[2] T. Metzger *et al.*, "Defect structure of epitaxial GaN films determined by transmission electron microscopy and triple-axis X-ray diffractometry," *Philosophical Magazine A*, vol. 77, no. 4, pp. 1013–1025, Apr. 1998, doi: 10.1080/01418619808221225.

[3] V. Srikant, J. S. Speck, and D. R. Clarke, "Mosaic structure in epitaxial thin films having large lattice mismatch," *Journal of Applied Physics*, vol. 82, no. 9, pp. 4286–4295, Nov. 1997, doi: 10.1063/1.366235.

[4] J. Neugebauer and C. G. Van de Walle, "Gallium vacancies and the yellow luminescence in GaN," *Applied Physics Letters*, vol. 69, no. 4, pp. 503–505, Jul. 1996, doi: doi:10.1063/1.117767.

[5] E. C. H. Kyle, S. W. Kaun, P. G. Burke, F. Wu, Y.-R. Wu, and J. S. Speck, "High-electron-mobility GaN grown on free-standing GaN templates by ammonia-based molecular beam epitaxy," *Journal of Applied Physics*, vol. 115, no. 19, p. 193702, May 2014, doi: 10.1063/1.4874735.

[6] T. Narita *et al.*, "Overview of carrier compensation in GaN layers grown by MOVPE: toward the application of vertical power devices," *Jpn. J. Appl. Phys.*, vol. 59, no. SA, p. SA0804, Nov. 2019, doi: 10.7567/1347-4065/ab4610.

[7] D. Haase *et al.*, "Deep-level defects and n-type-carrier concentration in nitrogen implanted GaN," *Applied Physics Letters*, vol. 69, no. 17, pp. 2525–2527, Oct. 1996, doi: 10.1063/1.117727.

[8] T. L. Tansley and R. J. Egan, "Point-defect energies in the nitrides of aluminum, gallium, and indium," *Phys. Rev. B*, vol. 45, no. 19, pp. 10942–10950, May 1992, doi: 10.1103/PhysRevB.45.10942.

[9] C. G. Van de Walle and J. Neugebauer, "First-principles calculations for defects and impurities: Applications to III-nitrides," *Journal of Applied Physics*, vol. 95, no. 8, pp. 3851–3879, Mar. 2004, doi: 10.1063/1.1682673.

[10] K. Saarinen *et al.*, "Gallium vacancies and the growth stoichiometry of GaN studied by positron annihilation spectroscopy," *Appl. Phys. Lett.*, vol. 73, no. 22, pp. 3253–3255, Nov. 1998, doi: 10.1063/1.122735.

[11] L. V. JØrgensen, A. C. Kruseman, H. Schut, A. V. Veen, M. Fanciulli, and T. D. Moustakas, "Investigation of Vacancies in GaN by Positron Annihilation," *MRS Online Proceedings Library (OPL)*, vol. 449, p. 853, ed 1996, doi: 10.1557/PROC-449-853.

[12] P. Bogusl/awski, E. L. Briggs, and J. Bernholc, "Native defects in gallium nitride," *Phys. Rev. B*, vol. 51, no. 23, pp. 17255–17258, Jun. 1995, doi: 10.1103/PhysRevB.51.17255.

List Publications and Conference Presentations

This is a selection of Eric Carlson's publications and conference presentations in III-V semiconductor growth and characterization while at Virginia Tech

[1]

Yunwei, Ming Xiao, Zhonghao Du, Lei Wang, Eric Carlson, Louis Guido, Han Wang, Lai Wang, Yi Luo, and Yuhao Zhang. "Activating Thick Buried P-GaN for Device Applications." *IEEE Transactions on Electron Devices* 69, no. 8 (August 2022): 4224–30. https://doi.org/10.1109/TED.2022.3186652.

Allen, Noah, Timothy Ciarkowski, Eric Carlson, Amrita Chakraborty, and Louis Guido. "Electrical Characterization of RuOx/n-GaN Schottky Diodes Formed by Oxidizing Ruthenium Thin-Films in Normal Laboratory Air." AIP Advances 10, no. 1 (January 2020): 015116. https://doi.org/10.1063/1.5125784.

Allen, Noah, Timothy Ciarkowski, Eric Carlson, and Louis Guido. "Characterization of Inhomogeneous Ni/GaN Schottky Diode with a Modified Log-Normal Distribution of Barrier Heights." Semiconductor Science and Technology 34, no. 9 (July 2019): 095003. https://doi.org/10.1088/1361-6641/ab3071.

Ciarkowski, Timothy, Noah Allen, Eric Carlson, Robert McCarthy, Chris Youtsey, Jingshan Wang, Patrick Fay, Jinqiao Xie, and Louis Guido. "Connection between Carbon Incorporation and Growth Rate for GaN Epitaxial Layers Prepared by OMVPE." Materials 12, no. 15 (January 2019): 2455. https://doi.org/10.3390/ma12152455.

Youtsey, Chris, Robert McCarthy, Rekha Reddy, Kamran Forghani, Andy Xie, Ed Beam, Jingshan Wang, et al. "Wafer-Scale Epitaxial Lift-off of GaN Using Bandgap-Selective Photoenhanced Wet Etching." Physica Status Solidi (b) 254, no. 8 (2017): 1600774. https://doi.org/10.1002/pssb.201600774.

Youtsey, Chris, Robert McCarthy, Rekha Reddy, Andy Xie, Ed Beam, Jingshan Wang, Patrick Fay, Eric Carlson, and Lou Guido. "Epitaxial Lift-off from Native GaN Substrates Using Photoenhanced Wet Etching." In 2017 International Conference on Compound Semiconductor Manufacturing Technology, CS MANTECH 2017, May 22, 2017

Louis J. Guido, Timothy A. Ciarkowski, Eric P. Carlson, and Noah P. Allen, "Behavior of arsenic in GaN at densities ranging from isovalent doping to dilute ternary alloys," International Workshop on Nitride Semiconductors (IWN 2016), Session F0.3 (Paper F0.3.05), Orlando, Florida, October, 2016.

Louis J. Guido, Eric P. Carlson, Timothy A. Ciarkowski, and Noah P. Allen, "Electronic properties of n-type and p-type GaN with isovalent arsenic co-doping," 6th International Symposium on Growth of III-Nitrides (ISGN-6), Session Tu-A (Paper A12), Hamamatsu, Japan, November, 2015.